Engineering Geology 317 (2023) 107054

Contents lists available at ScienceDirect

Engineering Geology

journal homepage: www.elsevier.com/locate/enggeo

28th September 2018 M_W 7.5 Sulawesi Supershear Earthquake, Indonesia: Ground effects and macroseismic intensity estimation using ESI-2007 scale

Sambit Prasanajit Naik [a,*], Asmita Mohanty [b], Valkaniotis Sotiris [c], Himanshu Mittal [d], Sabina Porfido [e,l], Alessandro Maria Michetti [f], Ohsang Gwon [g], Kiwoong Park [g], Asri Jaya [h], Ryan Paulik [i], Chuanyou Li [j], Takahito Mikami [k], Young-Seog Kim [g,*]

[a] Active Fault and Earthquake Research Institute, Pukyong National University, Busan 48513, South Korea
[b] National Institute of Advanced Studies, Indian Institute of Sciences (IISC) Bengaluru, Karnataka 560012, India
[c] Department of Civil Engineering, Democritus University of Thrace, 67100 Xanthi, Greece
[d] National Center for Seismology, Ministry of Earth Sciences, Govt. of India, New Delhi 110003, India
[e] ISA-CNR, Via Roma, 64-80100 Avellino, Italy
[f] Dipartimento di Scienza e Alta Tecnologia, Università dell'Insubria, Via Valleggio, 11, 22100 Como, Italy
[g] Department of Earth and Environmental Sciences, Pukyong National University, Busan 48513, South Korea
[h] Department of Geological Engineering, Hasanuddin University, Jl. Poros Malino KM.6 Bontomarannu, Gowa, South Sulawesi 92171, Indonesia
[i] National Institute of Water and Atmospheric Research (NIWA) Wellington, New Zealand
[j] State Key Laboratory of Earthquake Dynamics, Institute of Geology, China Earthquake Administration, Beijing, China
[k] Department of Urban and Civil Engineering, Tokyo City University, 1-28-1, Tamazutsumi, Setagaya-ku, Tokyo 158-8557, Japan
[l] Istituto Nazionale di Geofisica e Vulcanologia, Sezione di Napoli Osservatorio Vesuviano, Via Diocleziano 328, 80124 Naples, Italy

ARTICLE INFO

Keywords:
Sulawesi Earthquake
Indonesia
EEEs
ESI-07
ShakeMap
Seismic Hazard

ABSTRACT

The 28th September 2018 Sulawesi Supershear earthquake (M_W 7.5) was one of the deadliest earthquakes in the recent history of Indonesia causing ~4000 causalities. The earthquake caused a ~ 177 km long surface rupture along the Palu-Karo fault. Apart from surface rupture, the earthquake caused extensive earthquake environmental effects (EEEs) around the Palu-Donggala area of Central Sulawesi, Indonesia, which includes tsunami, coastal landslide, liquefaction, ground cracks and more than 7300 landslides in hilly areas. Initial post-event analysis and reports assigned a Modified Mercalli Intensity (MMI) of VII to VIII in Palu City and the surrounding area. Building damage and ground effects caused by the earthquake suggested that seismic intensity was understated. Here we applied the EEEs information from field survey data, published reports, and remote sensing tools to determine macroseismic intensity using the Environmental Seismic Intensity (ESI-07) Scale. The ESI-07 intensity derived from the ground effects suggests the maximum intensity of X-XI, which is 3–4° higher than the traditional intensity estimated by the United States Geological Survey (USGS) and the Indonesian Agency for Meteorology, Climatology, and Geophysics (BMKG). ShakeMaps were generated considering the ESI-07 values. The ShakeMap was compared with the instrumentally derived ShakeMap for the Palu earthquake, which proves that the ShakeMap prepared from the instrumental data or structural damage data is underrated. We argue that proper documentation of the EEEs is necessary for such damaging earthquakes for future earthquake hazard mapping and planning in the study area and other earthquakes in Indonesia. In addition, this will help in defining the on-fault and off-fault damage zone towards reducing the seismic risk of the Palu Donggala area.

1. Introduction

Traditional intensity scales such as Modified Mercalli (MM; Wood and Neumann, 1931); Medvedev-Sponheuer-Karnik (MSK; Medvedev et al., 1964); Arias intensity (I_A; Arias, 1970), European Macroseismic scales (EMS-98; Grünthal et al., 1998) incorporate various earthquakes induced effects on humans, buildings, and the environment, in order to understand the earthquake impact on society. These intensity scales (MM, MSK, EMS-98) mostly reflect the economic and cultural development of the affected region rather than the strength of the earthquake

* Corresponding authors.
E-mail addresses: sambitnaik@gmail.com (S.P. Naik), ysk7909@pknu.ac.kr (Y.-S. Kim).

https://doi.org/10.1016/j.enggeo.2023.107054
Received 28 March 2022; Received in revised form 10 January 2023; Accepted 18 February 2023
Available online 23 February 2023

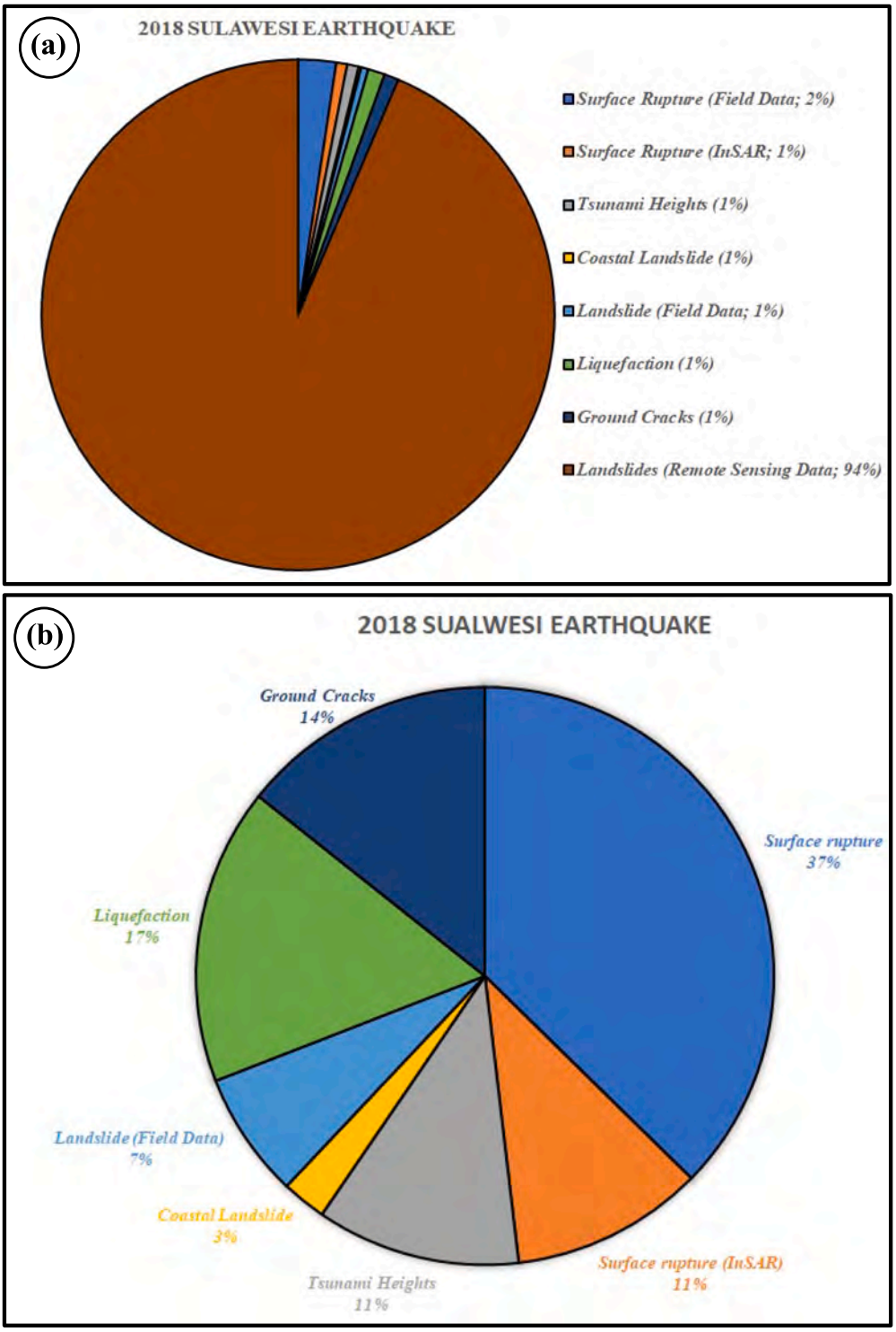

Fig. 1. Pie chart representing the Earthquake Environmental Effects (EEEs) for the 28th September 2018 Sulawesi earthquake, Indonesia for the generation of ESI-07 intensity map and ESI-07 ShakeMap (a) Shows the Pie chart for total 7537 number of data sets used, (b) Pie chart for all the datasets excluding the landslide data points extracted from remote sensing data.

(Papanikolaou and Melaki, 2017). The impact of the earthquake on the natural environment is being overlooked by these traditional intensity scales despite different upgradation with time (Sanchez and Maldonado, 2016; Papanikolaou and Melaki, 2017). The earthquake, impact on the natural environment was initially introduced in some of the traditional intensity scales (e.g. MSK64) but those scales were not able to differentiate the primary and secondary ground effects observed during an earthquake. This may be due to the complex nature of the earthquake's effects on the natural environment (Michetti et al., 2007; Papanikolaou and Melaki, 2017). Also, it has been noticed that seismic hazard analysis using the traditional intensity scales also may underestimate or overestimate the seismic hazard particularly for subduction zone earthquakes of Asia and South America, due to limited and incomplete macroseismic data, confusion over the source of the earthquake and significant modification of building codes in last 50 years (Villar-Vega et al., 2017). To overcome this problem, the environmental seismic

intensity (ESI-07) scale was introduced to calibrate the size of an earthquake by considering the quantitative analysis of EEEs (Michetti et al., 2004; Michetti et al., 2007; Serva et al., 2016). The ESI-07 scale solely considers the occurrence, size, and spatial distribution of the primary (surface faulting, coseismic upliftment or subsidence) and secondary effects (liquefaction, landslide, rock falls, ground collapse, tsunami, hydrological effects) caused by the earthquake. Unlike the traditional intensity scales, the ESI-07 scale is independent of human-induced effects. It allows to compare the intensity of recent and historical earthquakes in a particular region as well as earthquakes from different tectonic settings (Michetti et al., 2004; Porfido et al., 2007; Papanikolaou and Melaki, 2017; Huayong et al., 2019; Naik et al., 2020). The ESI-07 scale also has the upper hand over the traditional scales as ESI-07 allows us to estimate the seismic intensity more accurately in less habited areas and for the areas where the traditional intensity scale became saturated (for intensity level X-XI). Apart from this, the ESI-07 scale can predict the epicentral intensity considering the total area affected by the seismic events for which surface rupture is not observed (Silva et al., 2013; Serva et al., 2016). Due to this, ESI-07 scale has been applied for numerous seismic events worldwide (Serva et al., 2016; Papanikolaou and Melaki, 2017; Porfido et al., 2020; Nappi et al., 2021; Mavroulis et al., 2021; Velázquez-Bucio et al., 2021). The ESI-07 scale has been successfully integrated into paleoseismology, archeoseismology, and earthquake geology (Rodríguez-Pascua et al., 2011) for fault specific hazard assessment which will be useful for land use planning (Papanikolaou and Melaki, 2017; Naik et al., 2020). Some of the studies suggested the integration of the ESI-07 scale with faulting type, earthquake magnitude will be helpful for the development of earthquake attenuation relationship and ShakeMaps which may overcome the uncertainty in a developed attenuation relationship using traditional intensity scales (Silva et al., 2017). However, there are very few such studies reported from South-Asia or South-Eastern Asia with no case studies from Indonesia analyzing the seismic hazard using the EEEs. Indonesia has a long history of seismic hazards due to its geological settings with more than 62% of its population exposed to earthquake disasters (Jena et al., 2020). The country has recorded one of the highest earthquake death and injury rates due to earthquakes since 1990. 1996-Sulawesi, 2004-Sumatra, 2005 -Yogyakarta, 2006-West Java and West Sumatra, 2007-Bengkulu and West Sumatra, and 2009-West Java and West Sumatra are some of the damaging earthquakes (Wardani and Muntohar, 2013). The earthquakes listed here have caused the death of thousands of people and damaged half a million lifeline structures. Some of these earthquakes have also caused severe tsunamis (Wardani and Muntohar, 2013). Despite the long history of damaging earthquakes, no attention has been given to the proper documentation of ground effects caused by those seismic events, estimation of the ESI-07 scale, and its use in seismic hazard zonation in Indonesia. Following the above reason, the major goal of the present study are: (a) to expand the existing database of ESI-07 maintained by Istituto Superiore per la Protezione e la Ricerca Ambientale (ISPRA-Italy) from the Asian region where most of the data sets are from the Mediterranean or Europe, (b) to test the applicability, how the ESI-07 correlate with recent and historical seismicity for the same region in Indonesia, (c) to understand the role of local geology in the distribution of EEEs, ESI-07 scale has been applied for the very 1st time for any earthquake in Indonesia. In addition to these, an attempt has been made to prepare ShakeMap considering the ESI-07 values. The two-earthquake event which affected the Sulawesi region i.e. 1st January 1996 and 28th September 2018 Sulawesi earthquake were considered for the present study. The EEEs considered for the 1st January 1996 Indonesia earthquake mostly consider the secondary ground effects (Tsunami inundation heights) whereas the for the 28th September 2018 Sulawesi earthquake the EEs includes both primary (surface rupture) and secondary ground effects such as Tsunami, landslide, lateral spreading, liquefaction and ground cracks. Total 7537 number of observed and reported data sets were considered (Fig. 1a, b) for the present study to prepare the ESI-07 intensity map and ShakeMap. The result of the present study outlines the importance of documentation of EEEs and re-evaluation of seismic intensity for historical earthquakes in order to more accurate seismic hazard assessment of the study area and for other earthquakes and other regions of Indonesia. This study along with a reassessment of seismic intensity for the historical earthquakes and the recent earthquake in Indonesia will be helpful, to characterize the shaking intensity of modern and historical earthquakes, identify the potential sites for future paleoseismic investigations and develop a regional attenuation relationship between earthquake magnitude and ground effects as well as the development of a regional ShakeMap for Indonesia considering the EEEs. In addition, the distribution of EEEs may guide the development of an on-fault and off-fault deformation zone, which can be used for land use planning and more realistic seismic hazard estimation.

2. ShakeMap

ShakeMap is a product of the national (Indonesian Agency for Meteorology, Climatology, and Geophysics (BMKG) in the case of Indonesia) or international such as the United States Geological Survey (USGS) Earthquake Hazards Program in association with the local or regional seismic networks (Wald et al., 1999). ShakeMaps provide the ground motion Peak Ground Acceleration (PGA)/Peak Ground Velocity (PGV) maps of ground motion and shaking intensity for an earthquake. These ShakeMap are generally used by the local, regional as well as consultants for post-disaster response and recovery planning as well as for future earthquake hazard planning. These ShakeMaps are prepared from the recorded PGA or PGV and are not generally calibrated with the post-disaster damage survey (Silva et al., 2017) citing the urgency to achieve a rapid post-earthquake response. In addition, the ShakeMap prepared from the sparsely distributed seismic stations or seismic recording stations located at a distant location from the epicenter may underscore the ground motion parameter, hence the damage and post-disaster damage assessment. Besides, the ShakeMap is only available for recent earthquakes of the past few decades (only available for the first half of the 20th century) with technological advancement. Nevertheless, for historical earthquakes, still it relies on the macroseismic analysis based on the damage pattern observed which may be biased by the economic and cultural advancement of the location in historical time. To overcome this issue, recently some studies have been carried out towards improvement of the relationship between the intensity derived from the EEEs and seismic ground accelerations for historical as well as instrumental earthquakes (Rodríguez-Pascua et al., 2011; Rodríguez-Peces et al., 2011; Silva et al., 2017; Silva et al., 2023). Silva et al., 2017 developed the high-resolution ESI-07 ShakeMap using the EEEs for two historical earthquakes in SE Spain and compared it with the modern event as a calibration tool. The study suggested that the ShakeMap prepared from the ESI-07 provides a better definition of geological parameters. This kind of study is mostly confined in Europe, which indicates that more studies are required to test the applicability of the ShakeMap from EEEs from diverse geological settings and different earthquake mechanisms. Particularly for Indonesia where 62% of its total population are exposed to earthquake hazard with a prolonged history of damaging earthquakes, the ShakeMap prepared considering the EEEs may expand the window of hazard scenario for historical, ancient, and prehistoric earthquakes by digging the earthquake catalogs. So in this present study, an attempt has been made to prepare the ShakeMap using the ESI-07 values of the 2018 Palu earthquake using the Earthworm Software Module. The main reason to use the Earthworm software module is that it takes into account the surface rupture trace that is not included in the conventional ShakeMap generated by BMKG or USGS. The program ShakeMaps receives the intensity value information from the input file and saves the values of each place. With these stored values, the software module will perform the spatial interpolation calculation using inverse distance weighting (Yang et al., 2018; Mittal et al., 2019; Wu et al., 2019) to obtain a reasonable regional ShakeMaps.

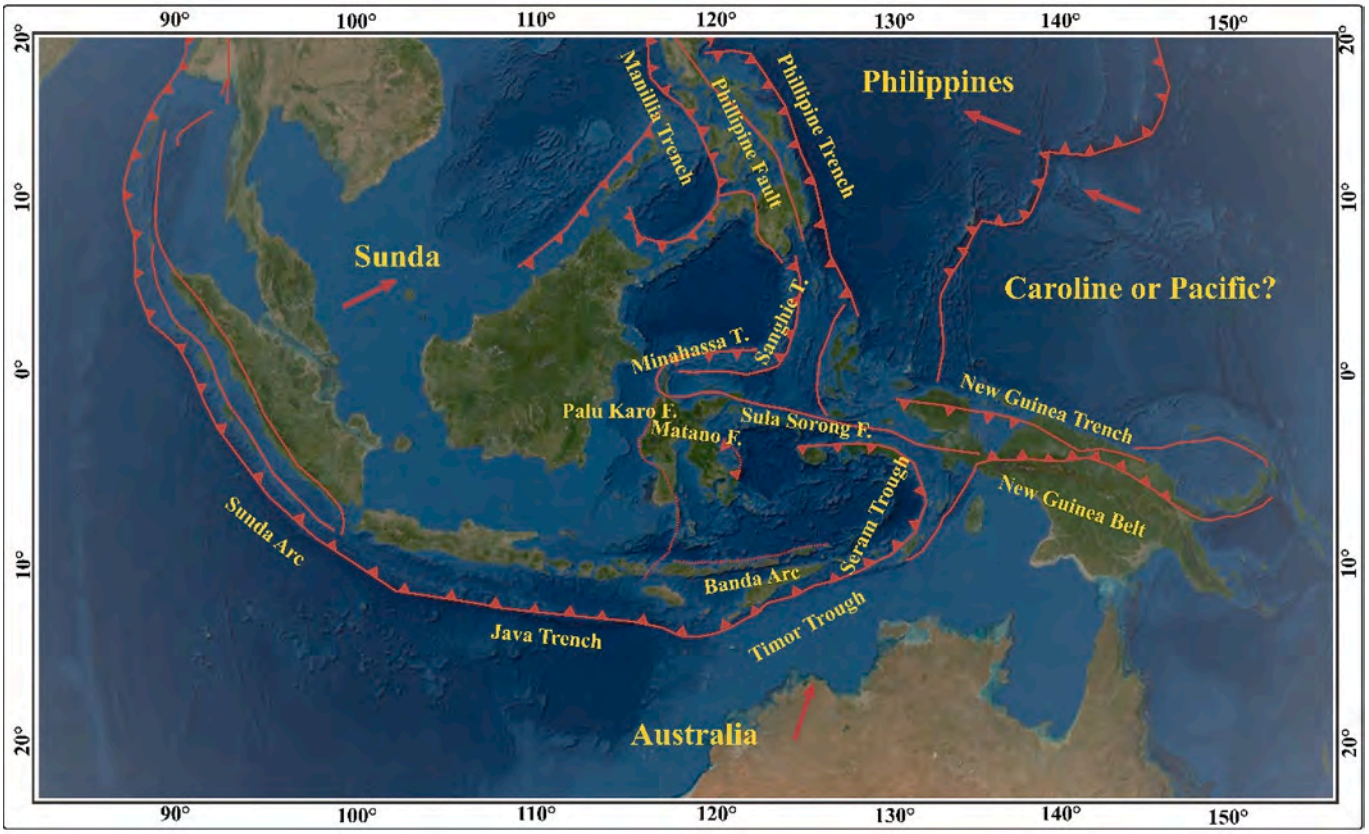

Fig. 2. Tectonics map of the Sunda–Australia–Philippine–Pacific region; red arrows indicate the direction of relative motion of the plates with respect to Eurasian Plates; modified from Socquet et al., 2006; Song et al., 2019; Image Source: Earth 3D Map, ESRI; http://earth3dmap.com/). (For interpretation of the references to color in this figure legend, the reader is referred to the web version of this article).

This methodology is followed in many studies (Legendre et al., 2017; Mittal et al., 2018; Yang et al., 2021). The ShakeMaps were compared with the BMKG and USGS ShakeMap. The ShakeMap prepared for the 2018 earthquake may symbolize the use of the ESI-07 scale with other traditional intensity scales for a more realistic earthquake hazard assessment. In addition, it may lead to the development of an empirical relationship to estimate the moment magnitude from the earthquake intensity distribution for historical earthquakes as well as for earthquakes occurring in an area having a very sparse modern seismic station network distribution.

3. Geological and tectonic settings

Sulawesi is located at the triple junction between the Indo-Australian, Philippine and Sunda Sea Plates in Southeast Asia (Hall and Wilson, 2000; Watkinson and Hall, 2017; Fig. 2). The Sulawesi Island moved towards NW with a clockwise rotation of about 4°/Ma due to its location which is wedged by the Australian Plate in the south and Philippine Plate in the east and resisted by buoyant Borneo continental crust in the west (Watkinson and Hall, 2017). Towards the north, the Celebes Sea Plate is being subducted under Sulawesi where the Minahassa Trench is accommodating the NW- directed movement of the Sula Block relative to the Sunda Plate. Due to the collision with the Banda and Philippine Sea plate in the east and roll-back subductions in the north, Sulawesi is subjected to trans-tension (Watkinson and Hall, 2017). The major active fault system of the area consists of the Palu-Koro and Matano Faults (Fig. 3a) which cuts obliquely the Sulawesi along NW-SE and act as trench-trench transform between the Minahassa and East Sulawesi Trenches (Watkinson and Hall, 2017).

The major structural features of the area are Palu-Koro Fault (PKF) (Fig. 3; Watkinson and Hall, 2017; Patria and Putra, 2020) which runs through Palu city. Despite sitting near the triple junction, the area possesses a low level of shallow seismicity around central Sulawesi (Bellier et al., 2001; Watkinson and Hall, 2017). Nevertheless, the tectonic geomorphology and recent paleoseismic studies suggest the area possesses a very high long-term slip rate i.e., 40 mm/yr on the PKF which matches with the present-day GPS measurements and is contrary to the observed seismicity (Bellier et al., 2001; Watkinson and Hall, 2017). Based on the geology and tectonic distribution, the Sulawesi is divided into 3 geological divisions i.e., (1) the Western Sulawesi Volcanic Arc, (2) the Eastern Sulawesi Ophiolite Belt and associated pelagic sedimentary deposits, (3) continental fragments derived from the Australian continent (Jaya et al., 2017). The Palu region is part of Sulawesi -a geological province composed of widespread K –volcanic and granitic rocks intruded into the Cretaceous to Paleogene metasedimentary rocks (Leeuwen and Muhardjo, 2005). The central part of the Palu basin is composed of Quaternary Molasses, Holocene fluvial deposits, and some patches of Quaternary marine terraces towards Donggala. The Quaternary molasses and Holocene fluvial deposits led the Palu basins more susceptible to higher amplification during the earthquakes and caused more damage (Fig. 3b).

4. Historical earthquakes and their ground effects

The Sulawesi region has a long history of earthquakes and tsunamis (Hamzah et al., 2000). According to the seismic catalog, Sulawesi has faced at least 14 tsunami events between 1820 and 1982 with a recurrence interval of 11 years (Hamzah et al., 2000). Out of these five earthquakes and tsunamis 1996 Sulawesi and the recent 28th September 2018 Sulawesi earthquakes are reported to be the most destructive events than others which were reported by the International Tsunami Survey Team (Pelinovsky, 1996; Pelinovsky et al., 1997; Putra et al.,

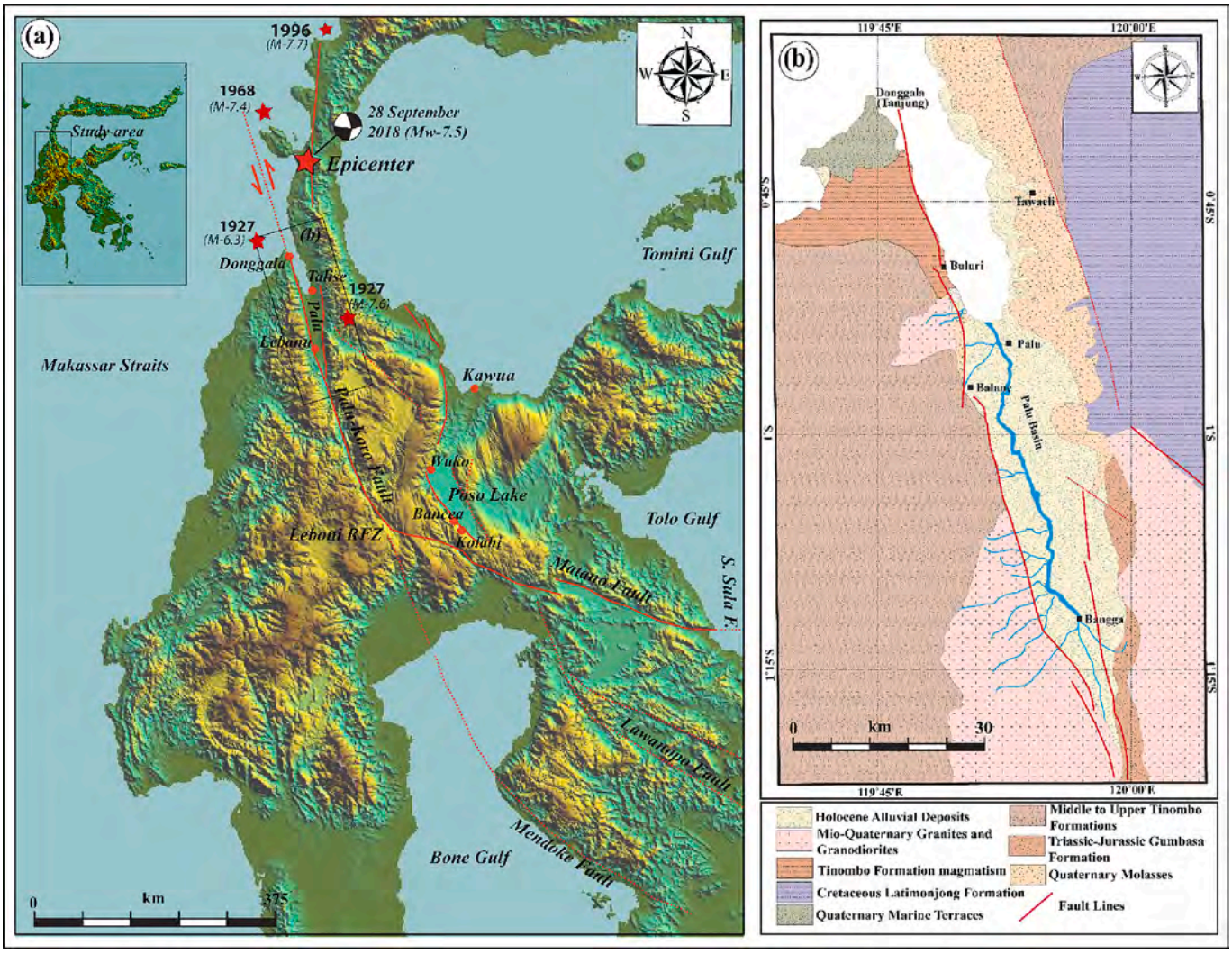

Fig. 3. (a) SRTM DEM showing the major active fault systems of the study area along with the USGS epicentral location of the 28th September 2018 Sulawesi earthquake (modified from Pelinovsky, 1996; Pelinovsky et al., 1997; Socquet et al., 2006; Song et al., 2019), (b) Geological map of the study area showing the distribution of major lithological units along with distribution of Quaternary marine terraces and molasses (modified after Sopaheluwakan et al., 1995).

2019; Omira et al., 2019; Paulik et al., 2019; Williams et al., 2020). The historical and present seismicity of these tsunamigenic events along the coastline of Sulawesi (Fig. 3a, Table 1) leave Sulawesi as one of the most vulnerable areas in terms of earthquake and tsunami hazards in Indonesia. The following part will describe some of the past damaging earthquakes that have affected the epicentral area of the 28th September 2018 Sulawesi earthquake.

4.1. 14th August 1968

The 14th August 1968 (0.2°N 119.8°E; M = 7.8) earthquake occurred along the northern coast of Sulawesi. This earthquake caused coastal land subsidence between Tandjung, Manirnbaha, and Sabang, along the Manimbaha Bay for about 2–3 m. The earthquake caused tsunami waves of 9-10 m high near Donggala. The land subsidence caused submergence in the Mapaga area soon after the earthquake. The tsunami inundated 500 m inland from the shoreline. The tsunami caused around 200 deaths, damage to 800 coastal homes, and flooding to large areas of coconut farming around the Donggala coast (Pelinovsky, 1996).

4.2. 1st January 1, 1996

On the 1st January 1, 1996 (0.83°N 120.01°E; M = 7.7) an earthquake occurred near the Makassar Strait along the Palu-Koro Fault. The epicenter was located around 25 km from the Tonggolobibi village and 180 km north of the Palu-Koro Fault. The moment tensor plot shows it was a reverse faulting event with a strike of 252° and a dip of 85°. The MM intensity of the earthquake was about X. The reported MMI values was resulted from the instrumental intensity from the USGS ShakeMap (https://earthquake.usgs.gov/earthquakes/eventpage/usp00079zv/executive). Due to the lack of tide gouge during that time, no instrumental data about tsunami waves around Sulawesi Island are available for this event. The earthquake caused a tsunami along the 120 km long coast of central Sulawesi out of which two regencies named Donggala and Buol Toli-Toli regency were severely affected. In Donggala regency, the Tonggolobibi village of Sojol district was badly affected. The tsunami run-up height was about 3-5 m, which inundated around 300 m inland from the coastline. The earthquake and tsunami caused the drifting of the houses nearly about 10 m from their original position along with the drifting of motor boats from the coast to inland about 250 m. About 300 houses were damaged in a Tonggolobibi village with 9 deaths. In Buol Toli-Toli regency, the Soni village was one of the most affected areas with tsunami wave heights of 1.5 m, which inundated 200 m inland from the coastline (Pelinovsky, 1996; Pelinovsky et al., 1997). The post-disaster survey by the Indonesian and Russian teams measured the tsunami heights along the 100 km long coastline of central Sulawesi.

Table 1
The list showing some of the damaging inland and offshore earthquakes affected Sulawesi (Pelinovsky, 1996; Hamzah et al., 2000; Gomez et al., 2000; Prasetya et al., 2001).

Region	Date of Earthquake	Lat./ Long.	Magnitude	MMI scale (USGS)	Max. Run Up height (m)
Sulawesi	29th Dec. 1829	–	–	–	–
Sulawesi	8th Feb 1845	–	–	–	–
Sulawesi	30th July 1907	–	–	–	–
Makassar Straight	1st Dec. 1927	−0.75/ 119.70	6.3	VII-VIII	15 m (approx.)
Banda Sea	1st Apr.1936	3.6/ 126.7	–	–	–
Makassar Straight	19th May 1938	1.0°/ 119.2°	–	VII-VIII	2–3 m
Central Sulawesi	20th May1938	−0.7/ 120.3	–	–	–
Central Sulawesi	22nd Dec. 1939	0.0/ 123.0	–	–	–
Sulawesi	29th April 1960	−0.5/ 121.50	–	–	–
Banda Sea	11th Apr.1967	−3.30/ 199.40	6.3	VII-VIII	8 m (approx.)
Celebes Sea	14th Aug. 1968	0.70/ 199.80	7.4	VII-VIII	10
Makassar Straight	23rd Feb. 1969	−3.10/ 118.50	6.1	VIII	10
Makassar Straight	06th Oct. 1972	−2.5/ 119.1	–	–	–
Makassar Straight	27th Feb 1974	−2.7/ 125.4	–	–	–
Celebes Sea	22nd Feb 1980	−1.61/ 124.93	–	–	–
Sulawesi	23rd Aug 1983	−2.31/ 120.97	–	–	–
N. Sulawesi	25th Oct.1983	1.08/ 121.05	–	–	–
Makassar Straight	8th Jan 1984	−2.77/ 118.72	6.7	VII	n.a.
Celebes Sea	17th Aug.1988	1.5/ 124.75	–	–	–
Celebes Sea	1st Jan 1996	0.74/ 119.93	7.9	VII-VIII	3.4
Peleng Island	4th May 2000	−1.29/ 123.59	7.6	VII-VIII	6

Considering the available anomalous tsunami wave heights, we have tried to evaluate the ESI-07 for the 1996 earthquake and compared it with the traditional intensity scale along with the 2018 Sulawesi earthquake (Pelinovsky, 1996; Pelinovsky et al., 1997; Table 2). The survey team reported vertical uplift of 0.70 m on Pangalaseang Island due to the earthquake based on the exposed coral reef edges (Pelinovsky, 1996; Pelinovsky et al., 1997). Considering the reported tsunami wave heights an ESI-07 intensity, of VIII was estimated for this earthquake, which shows a 2-degree difference from the MM intensity reported by USGS. The difference may be due to the less number of EEEs to validate the high degree of infrastructure damage.

4.3. 28th September 2018 Sulawesi Earthquake

The 28th September 2018 Sulawesi earthquake (local time 6:02:45 pm; epicenter: 0.256S and 119.846E; US Geological Survey) struck Palu City rupturing the Palu Koro fault nearly about 177 km (Jaya et al., 2019; Socquet et al., 2019; Wu et al., 2021; Natawidjaja et al., 2021). The earthquake is interpreted as a super shear earthquake as no aftershocks were reported after the mainshock along the Palu Koro fault with very simple faulting characteristics (Socquet et al., 2019). There are indications that the Palu Koro offshore fault section might have contributed to or been affected by the M_W 7.5 earthquake rupture

Table 2
Maximum tsunami wave heights recorded and the estimated ESI-07 and reported MM Intensity for the 1996 Sulawesi earthquake (Tsunami heights were taken from Pelinovsky, 1996; Pelinovsky et al., 1997; MM intensity values were taken from the USGS.

Location	Latitude	Longitude	Tsunami wave heights above MSL (m)	ESI-07 scale	MMI scale (USGS)
Pangalaseang Island	0°28′57.8”	119°54′25.1”	2.28	VIII	VI-VII
Mount	0°28′34.20”	119°55′50.9”	3.17	VIII	IX
Limbosu	0°28′26.4”	119°56′51.9”	2.81	VIII	VIII
Tonggolobibi	0°28′33.50”	119°57′27.8”	1.82	VIII	IX
	0°28′45.20”	119°58′35.6”	3.37		
	0°28′51.40”	119°58′41.3”	3.43		
Taipah	0°28′58.8”	119°59′30.0”	2.48	VIII	IX
	0°28′58.40”	119°59′51.4”	3.19		
	0°28′58.8”	119°59′52.0”	3.25		
	0°29′03.4”	120°00′11.9”	2.40		
Siboang	0°29′59.6”	120°01′38.8”	1.78	VIII	IX
Siwalempu	0°33′03.60”	120°02′19.9”	1.62	VIII	IX
Balukang	0°34′52.8”	120°02′13.0”	2.52	VIII	IX
Soni	0°45′57.20”	120°11′27.7”	1.79	VIII	IX
Dongko	0°49′15.3”	120°14′41.6”	2.39	VIII	IX
Simuntu	0°53′42.20”	120°14′14.6”	2.00	VIII	IX

(Bacqueset et al., 2020). The epicenter of the earthquake was located around 75 km north of Palu city. The focal mechanism of the earthquake suggests NNW left-lateral strike-slip with a normal faulting component (USGS, GCMT). This earthquake and tsunami are considered the most damaging earthquake in Indonesia after the 2004 Indian Ocean Tsunami (Widiyanto et al., 2019). Post-earthquake survey results and satellite image shows most of the tsunami impacts were limited to 300 m inland from the coastline of the Palu Bay area (Paulik et al., 2019). The earthquake caused extensive landslide, liquefaction, near-field tsunami, and ground cracks (Fig. 4), which caused the deaths of 2100 people, displaced 537,000 people, and damaged nearly 70,000 houses (ASEAN Coordinating Centre for Humanitarian Assistance on Disaster Management, 2018; https://ahacentre.org/search/). Considering the past and the present earthquake damage scenario and tsunami effects along Sulawesi Island, it can be inferred that Central Sulawesi is highly prone to earthquake-induced damage including tsunamis. Despite the long damage history, no attempt has been made so far for systematic mapping of the EEEs and preparing the ESI-07 map for the area which will eventually help for the better seismic hazard assessment and land use planning for the Palu basin and Sulawesi Island. So we have taken all the reported EEEs (both primary and secondary EEEs; Fig. 4) into consideration after the 28th September 2018 earthquake and an ESI-07 distribution map has been presented for the affected area.

5. Environmental effects of 28th September 2018 Sulawesi Earthquake

5.1. Primary effects

Primary co-seismic effects include permanent ground displacements that are surface rupture, regional coastal subsidence, or upliftment (Michetti et al., 2004; Michetti et al., 2007; Serva et al., 2016). They can be directly mapped in the field, as well as, can be traced from high-resolution satellite images (e.g. InSAR, UAV images) which have gained popularity in recent times (Lekkas and Mavroulis, 2015; Mavroulis et al., 2021). For the 28th September 2018 Sulawesi earthquake which shows more than ~177 km long surface rupture (Jaya et al., 2019; Socquet et al., 2019; Wu et al., 2021; Natawidjaja et al., 2021; Li et al., 2022), we have considered both the field observations and high-resolution satellite images (Sentinel-2) for the measurement of surface

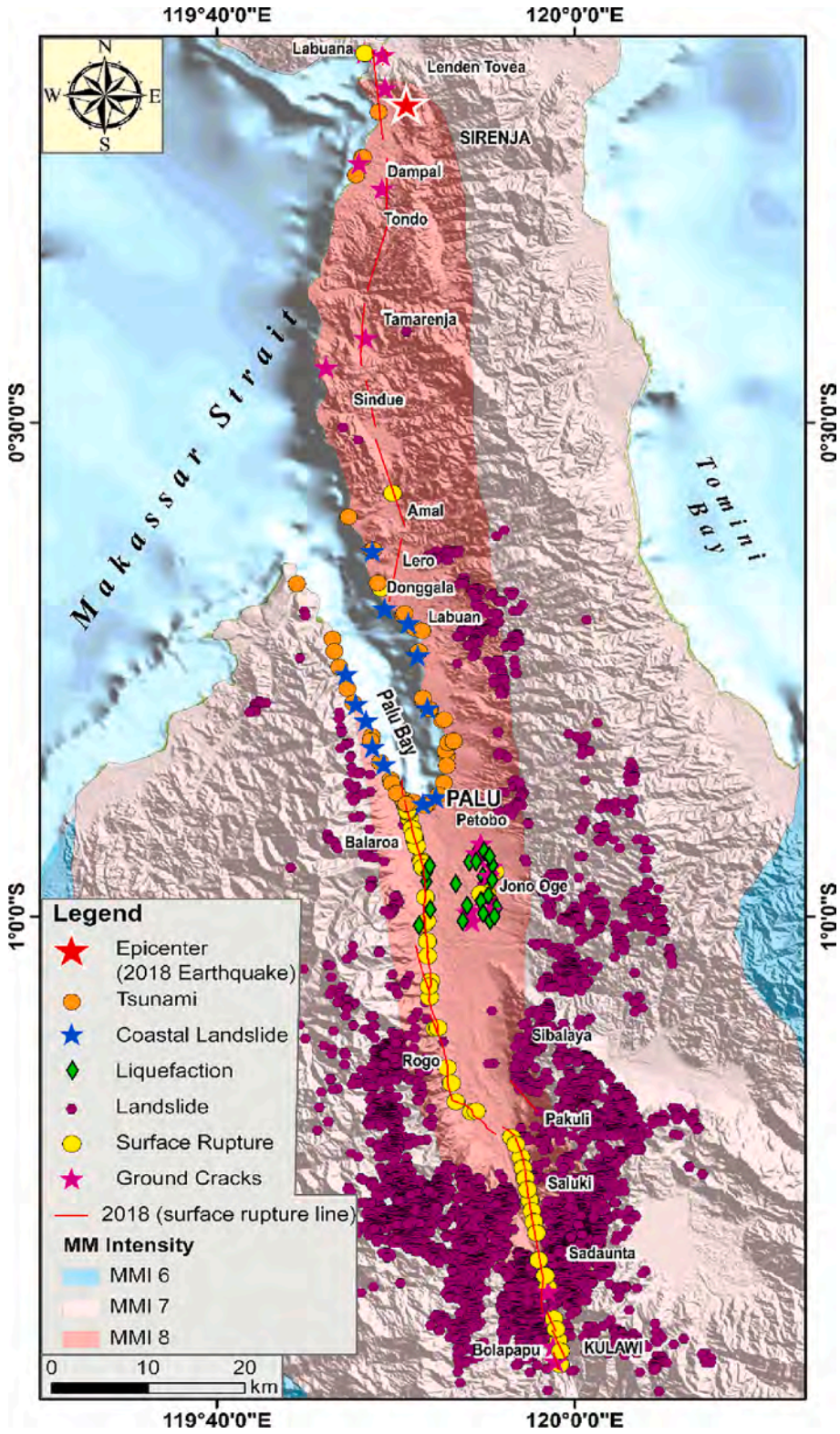

Fig. 4. A map showing the distribution of primary and secondary effects caused by Palu earthquake. The primary effects include primary and secondary surface rupture whereas the main secondary effects were tsunami, landslide, liquefaction, and ground cracks. The MMI values were taken from USGS.

offset due to the fault movement (Table 2-3; Fig. 4-6). The field measurement data were clustered at some locations depending upon the accessibility of the area. To overcome this and have a complete data set for the surface rupture to include in our analysis we have used the image correlation techniques using Sentinel-2 images. This technique has been successfully applied for tracing the surface rupture during recent damaging earthquakes around the world (Fielding et al., 2005; Wang et al., 2018). Pre and post-earthquake Sentinel-2 images (Sentinel-2 data procured 17th September 2018 and 2nd October 2018) were analyzed using *MicMac* software and used for tracing the surface rupture and offsets. Several swath profiles were taken along the surface rupture trace to measure the offset values at regular intervals along the Palu and

Table 3
Table shows the comparison between SIG intensity scale provided by Badan Meteorologi, Klimatologi, dan Geofisika (BMKG) https://www.bmkg.go.id/gempabumi/skala-intensitas-gempabumi.bmkg?lang=EN, and MM intensity scale provided by USGS (Source: Last accessed: 26th February 2022).

Skala Intensitas Gempabumi (SIG) (BMKG)	Observations	MM intensity scale	PGA (gal)
I	Not Felt	I-II	<2.9
II	Felt	III-V	2.9–88
III	Slight Damage	VI	89–167
IV	Moderate Damage	VII-VIII	168–564
V	Heavy Damage	IX-XII	> 564

Saluki segments of the fault (Fig. 5-6a-c). Our image correlation results indicate the rupture was rather simple and straight like a super shear earthquake (Valkaniotis et al., 2018; Socquet et al., 2019). The estimated surface offset values were validated from the field observations for the same locality (Fig. 6c). Both the field and satellite image-derived offset values were used for the ESI-07 estimation. Lateral offsets were observed at several locations such as Palu Barat, Balaroa, Marawola, Talise, Bolapapu, Pawunu, Pipa air, Kedondong, Diponegoro, Cemera, Rogo, Saluki Utara, Kedondong etc., (Fig. 4-7; Table S1-S2). The maximum offset values obtained from both field data and satellite data interpretation are about 5 to 6.6 m around Cemera Indah, Pewunu, Jln Padanjakaya, Tatanga, Baliase, Marawola, Lere, Palu Barat, Kabonena Balane, Donggala Kodi, Pewunu, Bomba and Sigi Regency whereas the minimum lateral offset observed is less than 1 m at some locations such as Marawola, Sigi Biromaru, Tatanga, Bolapapu, Labuan, Pakuli, Kulawi, Sibalaya. Near Sigi Biromaru, some traces of secondary rupture were traced infield as well as from satellite images. A total of 220 observation points were taken into consideration in assigning the ESI-07 value. The epicentral intensity can be estimated; through the empirical relationship using the total length of surface rupture that occurred taking into account the professional experience with the ESI-07 scale (Michetti et al., 2004).

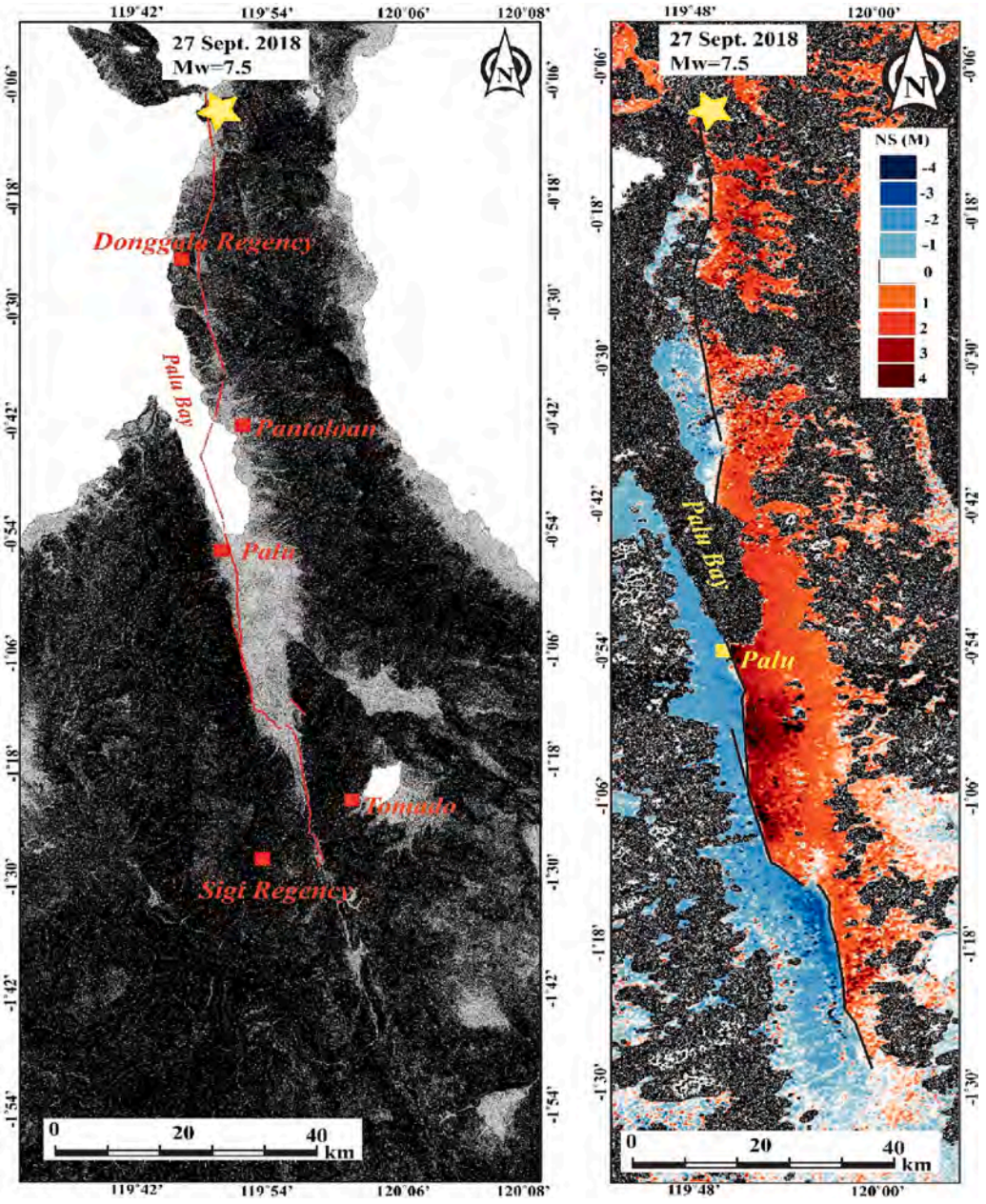

Fig. 5. (a) Surface rupture traces on the basis of field and satellite image analysis plotted on DEMNAS 8 m digital elevation model (tides. Big. go.id/DEMNAS); **(b)** image prepared from optical image correlation using Sentinel-2 (Copernicus/ESA) data showing horizontal displacement (N-S component) along Palu-Koro. Red color indicates the northward movement and blue color indicates southward movement; red (a) black (b) lines are the surface rupture traces for the 28th September 2018 Sulawesi earthquake; yellow star indicates the epicentral location of the earthquake. (For interpretation of the references to color in this figure legend, the reader is referred to the web version of this article).

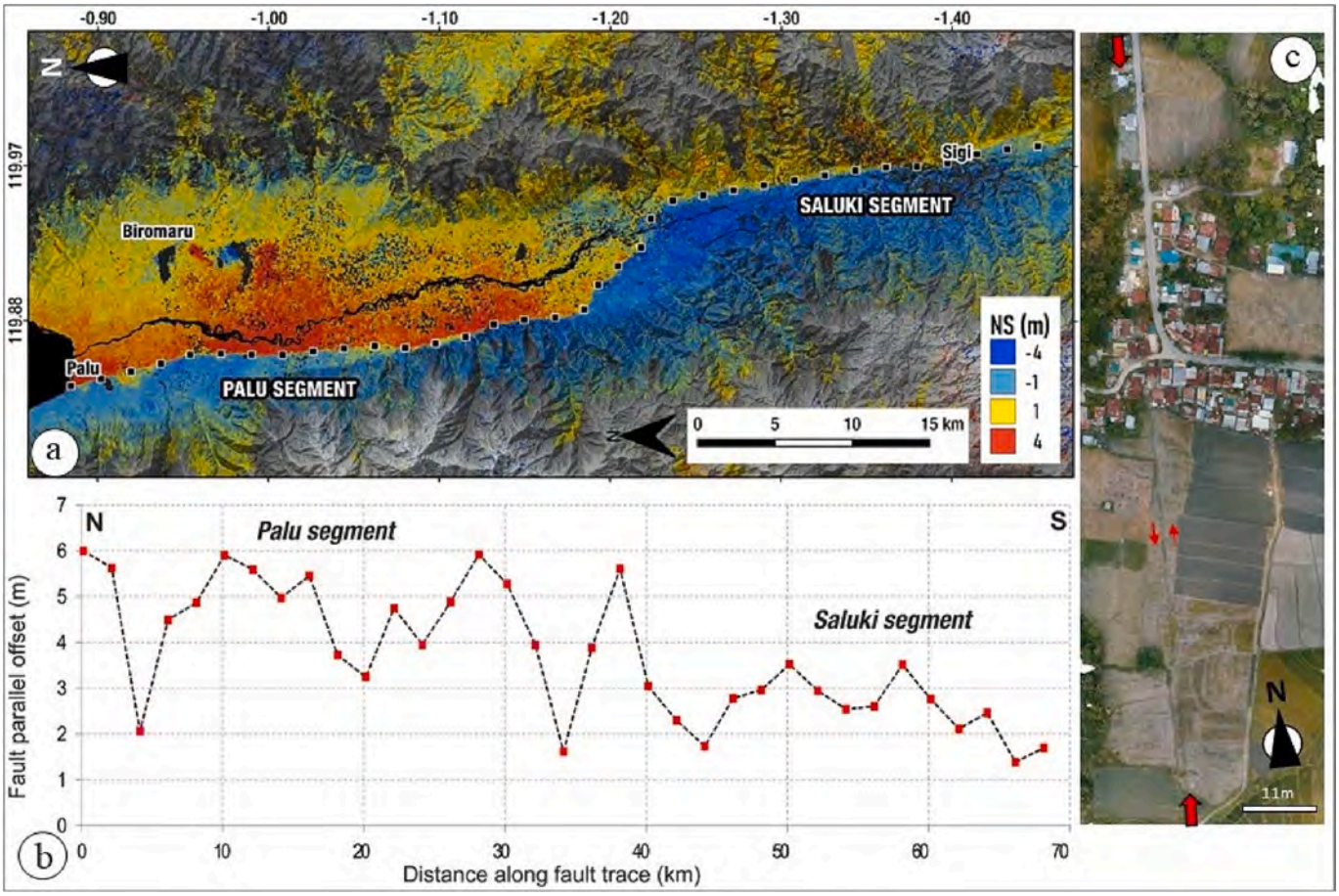

Fig. 6. **(a)** Detailed map of the co-seismic horizontal displacement field (North-South component) of the Palu and Saluki fault segment, obtained by optical image correlation using MicMac and Sentinel-2 imagery. Large uncorrelated patches (dark color) around Biromaru correspond to the large liquefaction slides on the eastern part of Palu basin. The black dots indicate the location of swath profiles taken for the measurement of fault parallel (strike-slip) offset along the Palu and Saluki Segment of the surface rupture; **(b)** the plot showing variation of horizontal offset (fault parallel displacement) along the surface rupture taken from field and image correlation; **(c)** UAV image showing the left lateral offset along Palu segment which was used to validate the offset measured from the Sentinel-2 imagery.

5.2. Secondary effects

Most of the secondary effects of the 28th September 2018 earthquake includes Tsunami, coastal landslide, landslides in hilly areas, liquefaction/water ponding, and lateral spreading that was observed between Sigi Regency, Palu city, and Donggala Regency. The detailed observed secondary effects have been described in the following sections.

5.2.1. Tsunami

The tsunamigenic 2018 Sulawesi earthquake caused extensive damage around the coastal area along Palu Bay. The Palu City and Donggala Regency were badly affected by the Tsunami. The tsunami washed away houses, bridges, mosques, and port structures along Palu Bay, Central Sulawesi Province. The Wani village, Pantoloan, Benteng village, Loli-Saluran village, Donggala, Tamunggu, Watusampu, Bulu Sigalari Bulu Kadia, North Ngapa, Tongge Bamba, Balaesang area were exposed to the tsunami (Pribadi et al., 2018; Cipta et al., 2018; PuSGeN, 2018, 2019; Arikawa et al., 2018; Muhari et al., 2018; Umar et al., 2019; Jaya et al., 2019; Widiyanto et al., 2019, Paulik et al., 2019; Mikami et al., 2019; Miyajima et al., 2019; Omira et al., 2019; Natawidjaja et al., 2021, Mason et al., 2021a, 2021b; Montgomery et al., 2021;). The farthest inundation distance from the coastline to the tsunami border on land is at the Layana site where inland inundation was about 511 m from the coastline. The highest point of the tsunami waves was found at the Tondo site with tsunami heights of more than 10 m. We have collected the tsunami wave heights and inland inundation distance from the coastline from ~55 locations (Table S3; Pribadi et al., 2018; PuSGeN, 2018, 2019; Faris et al., 2019; Widiyanto et al., 2019, Paulik et al., 2019; Mikami et al., 2019; Omira et al., 2019). Fig. 8 includes field photographs showing the tsunami inundation observed around Donggala, Palu, Pantoloan, and Silae area. Most of the data points were corrected to mean sea level using the tide gauge data from Mamuju and Pantoloan. Considering the above data, an attempt has been made to estimate the ESI-07 intensity. Recently several attempts have been made to quantify the tsunami effects in terms of intensity or magnitude (Papadopoulos and Imamura, 2001; Michetti et al., 2007; Lekkas et al., 2013; Lario et al., 2016). Out of which, the ESI-07 intensity scale, Tsunami Environmental Effect (TEE-16) scale are widely used intensity scales to quantify the effects of the tsunami. The ESI-07 scale consider the tsunami inundation height to classify the intensity (Michetti et al., 2007). However, the TEE-16 scale is the updated version of ESI-07 scale which consider the tsunami effects such as tsunami height, run-up height, possible flooded area, thickness of sedimentation by the tsunami waves (Lario et al., 2016). The TEE-16 scale follows the guideline of the ESI-07 scale and was validated by the recent tsunami events along with USGS instrumental intensity scale and ESI-07 scale. Both ESI-07 and TEE-16 scale have been applied to the 1755 Lisbon Tsunami, the 2004 Indian Ocean, 2006 Java, the 2010 Chile, the 2011 Tohoku events (Silva et al., 2017; Lario et al., 2016). For the present analysis, we have considered both ESI-07 and TEE-16 scales. From the analysis, it can be inferred that both ESI-07 and TEE-16 scales shows a 1–3-degree difference in macroseismic intensity between them. The

Fig. 7. Field photographs showing evidences for surface rupture of 28th September 2018 Mw 7.5 Sulawesi earthquake at (a) Amal (H = 40 cm; V = 7 cm); (b) Cemera I (H = 310 cm; V = 30 cm); (c) Rapadende (H = 420 cm; V = 20 cm); (d) Diponegoro (H = 240 cm; V = 27 cm); (e) Camera II (H = 340 cm; V = 20 cm); (f) Pakuli (H = 350 cm; V = 29 cm); (g) Dolobarat (H = 350 cm; V = 29 cm); (h) Balise-Biromaru (H = 370 cm; V = 40 cm); (I) Manunggal-Balise (H = 390 cm; V = 21 cm). The red arrow shows the sense of horizontal movement. (H=Horizontal displacement; and V=Vertical displacement of the ground surface). (For interpretation of the references to color in this figure legend, the reader is referred to the web version of this article).

intensity difference may be attributed to the difference in the classification of tsunami effects. The ESI-07 scale is independent of the earthquake type, whereas the TEE-16 scale includes the tsunami effects, considering the type of earthquakes. Though the TEE-16 scale has some advantages to make our interpretation uniform, we have considered the ESI-07 scale for our interpretations to keep consistency with our other ground effects.

5.2.2. Coastal landslides

During the 2018 Sulawesi earthquake, several places in Palu Bay show evidence of coastal landslides. It was distributed along the eastern and western sides of The Bay Area. Several researchers (Arikawa et al., 2018; Cipta et al., 2018; Widiyanto et al., 2019; Paulik et al., 2019; Mikami et al., 2019; Omira et al., 2019) reported the evidence of coastal landslide which is visible in pre and post-earthquake satellite images at around 14 locations along the Palu Bay. Coastal landslides occurred at Donggala, Loli-Pesua, Tamunggu, Benteng, Palu, Pantoloan, Tonga, Labuan along Palu Bay. Table S4 shows the locations of coastal landslides and the volume of the landslide observed during the earthquake. Fig. 9 shows the pre and post-earthquake satellite photos of the coastal landslide along Palu Bay, which indicates a significant amount of land loss occurred during the earthquake and Tsunami.

The area of the landslide was traced from the post-earthquake satellite images and polygon files were created for each landslide using the GIS platform. The volume of the landslide was calculated using the area volume relationship proposed by Larsen et al. (2010). Fig. 10 shows the coastal inundation during the earthquake around Donggala, Palu, Pantoloan, Talise, and Buluri.

5.2.3. Landslides

Slope failures associated with earthquakes are considered one of the common co-seismic environmental effects. Several recent studies (Keefer, 1984; Porfido et al., 2002; Del Gaudio and Wasowski, 2011), suggested that slope failure is one of the major components of earthquake hazard mitigation in seismically active areas. Hence, several approaches have been proposed to evaluate the earthquake-induced landslide hazard (e.g. Keefer, 1984; Del Gaudio and Wasowski, 2011; Wasowski et al., 2011). Several landslides caused by strong shaking were reported (PuSGeN, 2018, 2019; Cipta et al., 2018; Widiyanto et al., 2019; Jaya et al., 2019; Tunas et al., 2020; Zhao, 2021). Considering the above factors and hazards associated with landslides around the epicentral area, details about the landslides were collected from reporting literature, whereas some of the landslides were traced from Sentinel data and Landsat data. Most of the literature reported that landslides are occurring in hilly areas composed of Kambuno granite with a slope angle of 20°-50° (Zhao, 2021). The volume of the landslide was estimated using a similar formula used for the volume estimation of coastal landslide. Fig. 11 depicts the field photographs showing the landslides observed during the earthquake. Table S5 shows the details about the location, and the volume of landslide observed during the earthquake. The landslides were concentrated along the hilly regions of the Sigi Regency and the Donggala Regency. Some of the landslides were concentrated

Fig. 8. Field photographs showing the tsunami inundation around the (a) Palu city, (b) Donggala city, (c) Pantaloan, (d) Apung Palu Mosque, Palu, (e) damaged pavement due to tsunami in Buluri, (f) tsunami inundation mark in building wall in Silae.

around Oti, Sindue Tombusabora, Lero of Donggala Regency whereas most of the landslides were observed in Desa Sambo, Wisolo, Salua Village, Bangga village, Palolo, Pasaku, Gumbasa, Kulawi, Dolo Selatan, South Dolo area of Sigi Regency. It is well established that landslides produced by a strike-slip fault may distribute symmetrically on both sides of the fault (Fan et al., 2019). To understand this, we have analyzed the spatial distribution pattern of the seismically induced landslides mapped from the previous studies and landslides mapped from the remote sensing approach from the present study, which overlaps with the landslide mapped by Zhao, 2021. The spatial distribution of landslides suggests that the eastern side has a higher number of landslides than the western side of the surface rupture. The systematic analysis of the landslide distribution indicates that local geology plays a significant role in coseismic landslides rather than PGA (Zhao, 2021). The rock type (Kambuno Granite) was a dominant factor in landslide distribution. Apart from the rock type, the presence of en-echelon pattern normal fault on the eastern side of the 2018 surface rupture might have controlled the distribution of landslides on either side which resulted the higher number of landslides on the eastern side than on the west side of the surface rupture (Fig. 12). Some numerical and field-based studies suggested that step like slopes could locally affect the seismic ground motion by causing topographic amplification (Qi et al., 2021). The detailed mapping of the landslides and their dimension will help in defining the off-fault avoidance zone for further infrastructure development projects to minimize the seismic hazard.

5.2.4. *Liquefaction and lateral spreading*

During the Palu earthquake, severe damage was occurring around Balaroa, Petobo, Sigi Biromaru, and Sibalaya. The liquefaction-induced slide caused extensive building damage and the death of people. Extensive ground cracks and sand boil were observed along these large-scale liquefactions induced slides. In addition, several isolated sand boils were seen along the rice farms around Petobo, Sigi Biromaru, and Sibalaya. We have collected the reported dimensions of liquefactions from reporting post-earthquake survey reports and post-earthquake satellite images around Balaroa, Petobo, Sigi Biromaru, and Sibalaya (Fig. 13; Table S6) and used them for the ESI-07 assessment.

5.2.5. *Ground cracks*

Soon after the earthquake, ground cracks developed in several places around the epicentral area. Most of the ground cracks were noticed on gently sloping (1–2°) flat lands and rice farms (Bradley et al., 2019; Jaya et al., 2019). The ground cracks developed near Petobo, Lolu, Sigi Biromaru, and Balaroa were densely distributed. At some locations, cracks were spotted in paved and concrete roads. The reported ground cracks dimensions were compiled from the published papers, and reports, and traced the ground cracks from the post-earthquake satellite images and in the field, to access the ESI-07 values. Ground cracks were noticed around Labuana, Balaesang, Lenden Tovea, Dampal, Tondo, Tamarenja, Sindue, Saduanta, Leon, Boladangko, Birobuli Utara, Petobo, Lolu, Sigi Biromaru, and Karawana around the epicentral area (Fig. 14; Table S7).

6. ESI-07 Scale Estimation and ShakeMap

6.1. *ESI-07 Scale Estimation*

Considering the quantitative information of the earthquake-induced ground failures caused by the 28th September 2018 Sulawesi earthquake, the macroseismic intensities were estimated using the methodology pf ESI-07 scales provided by Michetti et al., 2007. A total of 7413 data points of both primary and secondary effects covering an area of ~3700 sq. km were used (Fig. 1, Fig. 4). We have selected the ESI-07 scale as it is solely based on the environmental effects and is consistent with the historical seismicity and its ground effects (Papathanassiou et al., 2017; Silva et al., 2019; Naik et al., 2020; Porfido et al., 2020). The computed degrees of epicentral intensity (I_0) for the 2018 Sulawesi earthquake considering the length of the surface rupture observed during the earthquake which is ~177 km and maximum vertical displacement of 6.6 m, the I_0 is in agreement with the ESI-07 of X-XI based on environmental effects. The empirical relations between epicentral intensity (I_0) and surface faulting parameters were used for the evaluation of the degree of I_0 for the 2018 Sulawesi earthquake using Eq. 1 and Eq.2 proposed by Michetti et al., 2004.

$$I_0 = 0.5503 \times Ln\,(\text{Surface Rupture Length}) + 7.861\ (\text{X} - \text{XI}) \quad (1)$$

Fig. 9. Pre and post-earthquake Google Earth image showing coastal land loss during the earthquake at (a) Loli, (b) Buluri, (c) Lere, (d) Labuan around Palu bay (Image source: https://earthengine.google.com/).

$$I_0 = 0.5786 \times Ln\ (\text{Maximum Displacement}) + 9.51\ (X - XI) \quad (2)$$

The ESI-07 values were compared with the BMKG and MM intensity. From the ESI-07 distribution, map it can be observed that the maximum intensities of X-XI were observed considering the surface rupture whereas considering the secondary ground effects a maximum intensity of IX-X was assigned around the epicentral area. Based on the primary and secondary effects, ESI-07 of XI were assigned for the locations around Jin Camera Indah, Kulawi, Balaroa, Dolobarat, Palu, Balane, Pasaku, Pakuli, Sigi Regency area, whereas the ESI-07 of IX-X were assigned for locations around Jono Oge, Sigi-Biromaru, Tatanga, Bolapapu, Lobana, Amal, Lero, Labuan, Loli Saluran, Kulawi, Beka, Bomba, Padende, Kalukubla, Mpanau, Biromaru, Lolu, John Oge, Sidera Karawana, Petobo Sadaunta, Tongkulawi, Boladangko, Birobuli, Longaleso and Kotarindau (Table 4, Table S1-S7; Fig. 15). Similarly, ESI-07 of VIII were assigned to Lere, Besusu Barat, Talise, Lero, Tanjung Padang, Lende, Donggala, Loli Saluran, Palu, Dupa, Labua, Towaja, Gumbasa, Oti. The ESI-07 values of VII were assigned to the Lero area considering the observed secondary effects (Table 4, Table S1-S7, and Fig. 15). Considering the tsunami heights for estimating the intensity, ESI-07 of

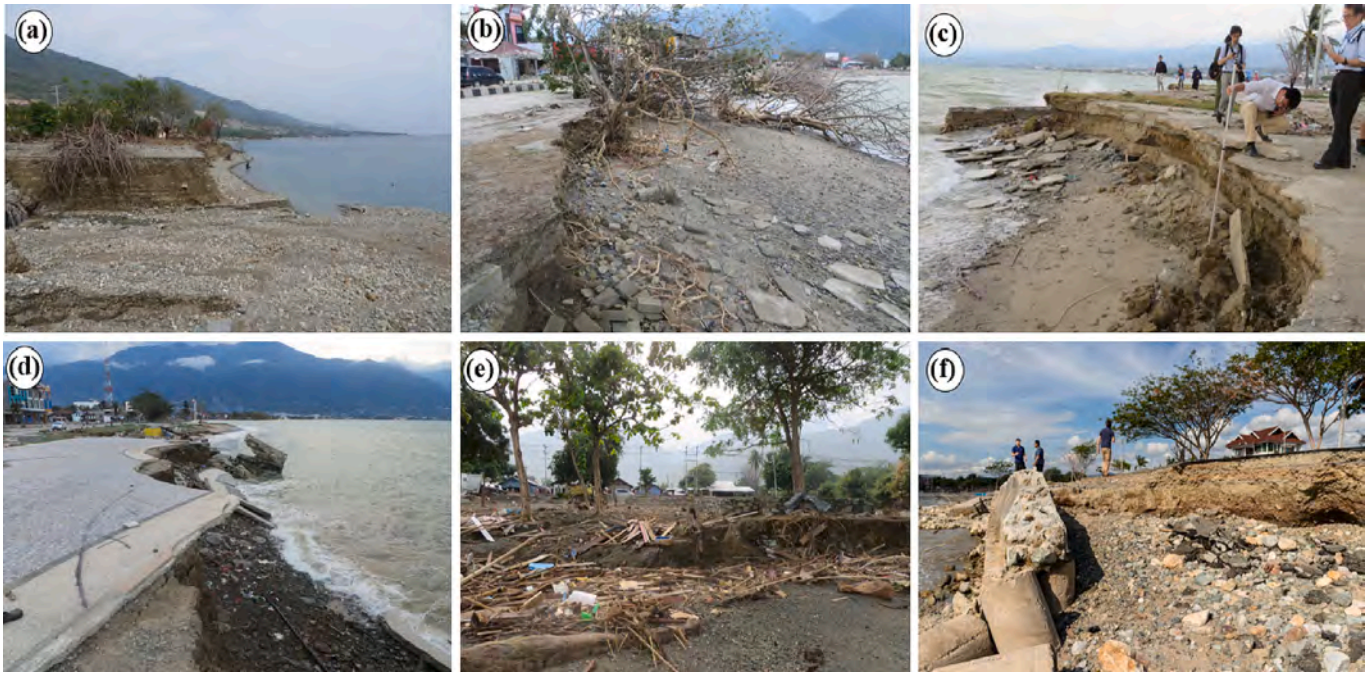

Fig. 10. Field photographs showing the land subsidence /land mass loss during the earthquake around (a) Benteng, (b) Lere, (c) Talise, (d) Mamboro, (e) Labuan, (f) Pantoloan.

X-XI was assigned to some of the areas, whereas the minimum intensity of VIII was assigned to some of the areas depending upon the inundation area and height.

To make sure that our ESI-07 intensity estimation considering the tsunami heights was assessed correctly, the ESI-07 scale was compared with the TEE-16 scale. Both scales provide similar intensity values. There is a 1 degree of intensity difference between the ESI-07 and TEE-16 scales. Despite this difference to make our interpretation uniform, it was decided to use the ESI-07 scale rather than TEE-16. The ESI-07 scale estimated using the EEEs was compared with other traditional intensity scales such as Skala Intensitas Gempabumi (SIG) intensity scale provided by BMKG, and the MM intensity scale from the USGS intensity scale. SIG is a five-level scale (I-V) and assigns the intensity considering the impact of an earthquake on Indonesian buildings. The MM intensity scale and SIG intensity scales are interrelated but the SIG intensity scale was calibrated to damage pattern observed in typical buildings in Indonesia (https://www.bmkg.go.id/gempabumi/skala-mmi.bmkg). The relationship between the SIG intensity scale provided by BMKG and MM intensity scale provided by the USGS is shown in Table 3.

We have considered both the scales to compare with the ESI-07 scale considering the wide acceptance of these two traditional scales in Indonesia and their correlation in between. Also, the MMI intensity or SIG intensity scale mostly relies on structural or instrumental data which may underestimate or overestimate the seismic intensity considering the economy-social development of a region. This kind of uncertainty was observed during the two recent earthquakes in Taiwan where two earthquakes of the same magnitude shows different PGA and different damage patterns (Wu et al., 2019).

The comparison of the ESI-07 scale with the SIG scale and MM intensity scale indicates that the ESI-07 scale is 3–4° higher than the traditional intensity scales (Table 4; Table S1-S7). The difference may be due to the localized seismic stations around the epicentral area. Apart from that both the SIG and MM intensity were estimated from the PGA and PGV values which were not calibrated according to the structural damage pattern observed after the earthquake. Also, the ESI-07 intensity were compared with the MM intensity estimated by Cilia et al., 2021 which includes the building damage data collected after the earthquake (Fig. S1). The MM intensity estimated from the field data suggests MM intensity value varies between V-X. The MM intensity estimated by Cilia et al., 2021 is 1–3 lower than the ESI-07 intensity values. The intensity distribution map prepared by Cilia et al., 2021 (Fig. S1) shows very scattered distribution of intensities around the Palu city, which may be due to the variation of local geology and distribution of heterogeneous building types (related to different building standards). Also due to the saturation of the traditional intensity scales for intensity X-XII, (Michetti et al., 2004, 2007) it is difficult to differentiate the damage pattern, hence assigning the appropriate intensity. However, the ESI-07 value shows a good correlation between the primary and secondary effects observed around the epicentral area.

To confirm the credibility of the ESI-07 scale application in the study area, we have estimated the ESI-07 and MM intensity for the 1996 Sulawesi earthquake that caused the tsunami around Sulawesi. We have made the intensity estimation using the inundation heights, which suggest the maximum ESI-07 was VIII, whereas a MM intensity value was X. Despite limited data sets and only tsunami data being used for this, this shows the 2-degree difference between these two scales. This comparison suggests the integration of EEEs with structural damage data may give more precise intensity distribution and seismic hazard for the study area and elsewhere in Indonesia.

6.2. *ShakeMap for the 2018 Palu earthquake*

ESI-07 ShakeMap (Fig. 16 a) has been generated for the 2018 Palu earthquake with the aim to use the EEEs for historical or modern earthquakes in Indonesia as well as areas of similar tectonic settings with an exemplary number of EEEs. The ShakeMap for the Palu Supershear earthquake (Fig. 16a) shows higher intensity (XI-X) along the surface rupture within the Palu Basin and lower intensity (VII-VIII) in hilly areas where small to large landslides were observed. Also, higher intensity values of VIII-IX were observed around the epicenter of the earthquakes. The ShakeMap also indicates the isolated patches of higher intensity within the lower intensity values which indicate the role of local geology in shaking intensity which is taken as uniform in BMKG or USGS ShakeMap (Fig. 16b-c). The shape of shaking intensity contours in BMKG or USGS ShakeMap is mostly controlled by the structural damage data. BMKG ShakeMap (Fig. 16b,c) shows the maximum intensity of VIII

Fig. 11. Observed landslide during the earthquake around (a) Walandano; (b) Lenden Tovea; (c) Rogo; (d) Tamarenja; (e) Amal; (f) Saluki.

around the Palu coast as it was badly affected by the tsunami and for some areas around Balaroa, Petobo, Sigi Biromaru as most of the house was washed out by liquefaction-induced lateral spreading. The USGS ShakeMap shows higher shaking intensity of VIII for the areas along the Palu-Karo Fault. Both the BMKG and USGS ShakeMap show lesser shaking intensity than the ESI-07 ShakeMap. This may be due to the lack of field validation of the damage observed for the BKMG and USGS ShakeMap. Also, the methodology involved in the formation of USGS ShakeMap overrules the topographic amplification and it overestimates the site condition for flat areas or areas having less thick quaternary sedimentary covers (Silva et al., 2017). The BMKG ShakeMap also adopts a similar workflow as the USGS ShakeMap where both the ShakeMap does not include the primary effects (surface rupture) for the generation of an intensity map. Therefore, the shaking intensity for the 2018 event has been understated by both the ShakeMap. The ESI-07 ShakeMap prepared from the present study is calibrated with the field evidence and it includes both the primary and secondary effects and may represent a more realistic shaking intensity scenario. This indicates that the ESI-07 ShakeMap can be integrated with the traditional damage-based intensity data as one of the major objectives of the ESI-07 Scale (Michetti et al., 2007; Silva et al., 2017; Silva et al., 2023).

7. Discussions

The 2018 Sulawesi earthquake caused extensive environmental effects, including a 177 km long surface rupture along the Palu-Karo Fault and secondary effects such as coastal landslide, tsunami, and slope failure in hilly regions, liquefaction and lateral spreading, ground cracks. A tsunami is reported during several historical earthquakes in the study area, but not well-documented environmental effects. This indicates the importance of documentation of EEEs to evaluate the macroseismic intensity of historical earthquakes in the region. Based on the collected EEEs using field surveys, Seninel-2 data, and other high-resolution satellite images, the macroseismic intensity of the 2018 Sulawesi/ Palu earthquake was estimated using the ESI-07 intensity scale. Considering the total area affected and primary effects, it can be inferred that the epicentral intensity for the 2018 Palu earthquake is to be I_0 = XI ESI-07. It can be noted that some areas of the epicentral area are directly related to site effects and do not represent the exact macroseismic intensity values. The liquefaction-induced flow landslide

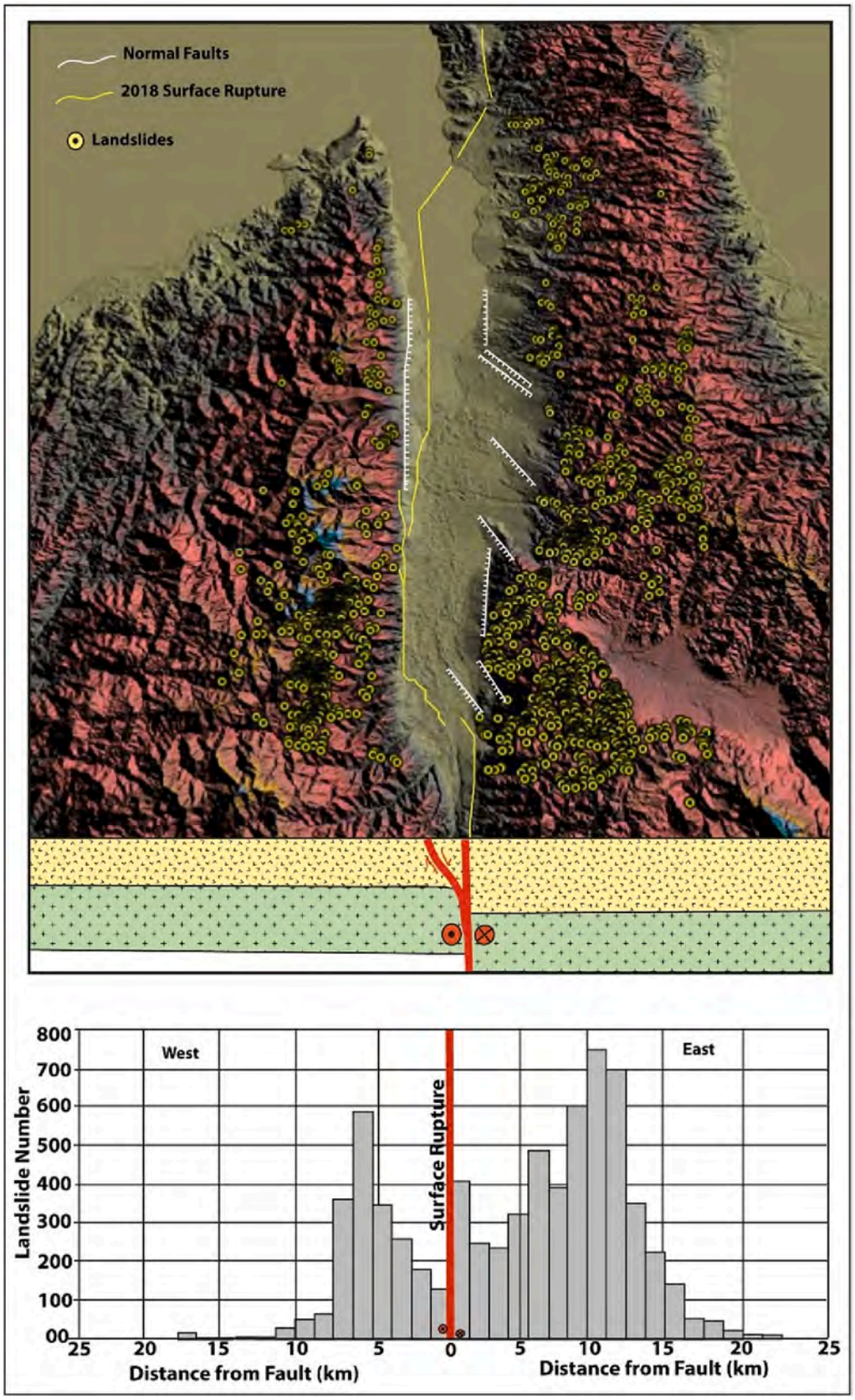

Fig. 12. Landslide distribution across the surface rupture of the 2018 earthquake indicates the role of complex fault system for the spatial distribution of the landslides (modified from Zhao, 2021).

Fig. 13. Field and satellite photos showing evidences of liquefaction and damaged houses due to liquefaction induced lateral spreading around Petobo, Sigi Biromaru and Sibalaya (Google Earth image source: https://earthengine.google.com/).

observed around Petobo, Biromaru, and Dolo areas were not considered in the macroseismic intensity estimation. Only the sand boil dimensions were considered in the macroseismic intensity estimation.

In this study, the field measurement data were integrated with space technology to test the accuracy of satellite data in macroseismic intensity estimation. Some recent studies suggested (Mavroulis et al., 2021) that the macroseismic intensity estimation using space technology offers higher intensity than the estimated intensity that relies on field measurements. In this case, we have used the descending and ascending Sentinel-2 data procured on the 17th of September 2018 and the 2nd of October 2018 to measure the tectonic displacement. The measured displacement values show a good match with the displacement values measured from the field and localized UAV images. The macroseismic intensity values are almost the same for both derived from the field measurements and InSAR measurements. This indicates the InSAR data and high-resolution satellite images could provide crucial information for developing macroseismic intensity estimation in seismic hazard analysis in the Indonesian region, as well as elsewhere in the world. Similar observations were made for the 2014 Cephalonia earthquakes in Greece where the InSAR data were used for the macroseismic

Fig. 14. Field photographs showing the ground cracks observed during the 2018 Palu earthquake around (a) Dampal; (b) and (e) Tondo; (c) Tamarenja and (d) Jono Oge, (e) Pakuli, (f) Amal.

intensity estimation (Papathanassiou et al., 2017).

The estimated ESI-07 values were compared with the SIG intensity and MM intensity scales which suggests that the ESI-07 intensity scale is 3–4° higher than the traditional intensity scale. This may be because the traditional intensity scales were not calibrated with the post-disaster structural damage data. The difference in the intensity between the traditional and ESI-07 scales indicates the integration of EEEs with structural damage data should be used for seismic hazard estimation for the study area and other damaging earthquakes in Indonesia.

ESI-07 ShakeMaps were prepared for the Palu earthquake considering both the primary and secondary effects which show a completely different shaking intensity scenario than the USGS and BMKG ShakeMaps, with higher shaking intensity along the observed surface rupture. This indicates the proper documentation of EEEs along with the structural damage data is required for calibration of the local intensity map and a better seismic hazard estimation. This also indicates that the ShakeMap can be prepared for the historical earthquakes in Indonesia or the areas having a well-documented catalog of EEEs.

The ESI-07 for the 1996 Sulawesi earthquake was also compared to the ESI-07 intensity for the 2018 Sulawesi earthquake. There is a one to two-degrees difference in the ESI-07 intensity, whereas the MM intensity gives almost similar values. This difference may be due to the difference in magnitude, location of the epicenter, and huge modification in the landscape during this period with growing urbanization. This comparison suggests further examination of similar cases and reevaluation of seismic intensity to have a more reliable seismic hazard zonation for

Table 4
Estimated ESI-07 intensity for different locations considering the maximum ESI-07 intensity observed based on EEEs. From this table, the maximum observed ESI-07 intensity values were taken despite of more than one values of ESI-07 intensity were reported to make the table more effective and compact.

Location Name	Latitude	Longitude	EEEs type	ESI-07 scale	MMI Scale (USGS)
Cemara Indah	−0.900084218	119.8461562	Surface rupture	XI	VIII
Marawola	−0.98008	119.8611	Surface rupture	XI	VIII
Jono Oge	−0.955040501	119.9257904	Surface rupture	IX-X	VIII
Sigi Biromaru	−0.954256877	119.9258301	Surface Rupture	IX-X	VIII
Tatanga	−0.909611173	119.8482159	Surface Rupture	IX-X	VIII
Kulawi	−1.347272163	119.9663116	Surface rupture	XI	VIII
Palu Barat	−0.909448061	119.8458507	Surface rupture	IX	VIII
Jin Padanjakaya	−0.9225576	119.8513659	Surface rupture	XI	VIII
Balaroa	−0.9088	119.84023	Surface Rupture	XI	VIII
Diponegoro	−0.88331	119.84122	Surface Rupture	XI	VIII
Talise	−0.882	119.84122	Surface rupture	XI	VIII
Dolo Barat	−1.02462	119.86256	Surface rupture	XI	VIII
Labuana	0.1258°	119.8043°	Surface rupture	IX-X	VIII
Amal	−0.5713°	119.8302°	Surface Rupture	IX-X	VIII
Lero	0.6340°	119.8119°	Surface Rupture	IX-X	VIII
Labuan	0.6697°	119.8218°	Surface rupture	IX-X	VIII
Lasoso	0.8888°	119.8431°	Surface rupture	XI	VIII
Asam	0.8939°	119.8445°	Surface rupture	XI	VIII
Kedondong	0.8968°	119.8453°	Surface Rupture	XI	VIII
Cemara	0.9003°	119.8456°	Surface Rupture	XI	VIII
Padanjakaya	0.9225°	119.8514°	Surface rupture	XI	VIII
Munuggal-Baliase	0.9424°	119.8568°	Surface rupture	XI	VIII
Rarapadende	0.0125°	119.8601°	Surface rupture	XI	VIII
Dolobarat	1.0259°	119.8625°	Surface Rupture	XI	VIII
Rogo	1.1865°	119.8887°	Surface Rupture	XI	VIII
Pakuli-Sibalaya	1.2304°	119.9453°	Surface rupture	XI	VIII
Saluki Utara	1.2763°	119.9564°	Surface rupture	XI	VIII
Tongkulawi	1.4314°	119.9840°	Surface rupture	X	VIII
Boladangko	1.4508°	119.9823°	Surface Rupture	IX-X	VIII
Silae	−0.8835	119.8415	Surface Rupture	XI	VIII
Lere,Palu Barat	−0.8843	119.8418	Surface rupture	XI	VIII
Kabonena	−0.8879	119.8429	Surface rupture	XI	VIII
Donggala Kadi	−0.8940	119.8446	Surface rupture	XI	VIII
Duyu	−0.9107	119.8487	Surface Rupture	XI	VIII
Balise	−0.9424	119.8569	Surface Rupture	XI	VIII
Marawola	−0.9447	119.8574	Surface rupture	XI	VIII
Pewunu	−1.0246	119.8625	Surface rupture	XI	VIII
Kabonena	−0.8882	119.8429	Surface rupture	XI	VIII
Lere	−0.8928	119.8442	Surface rupture	XI	VIII
Labua	−0.6676	119.8200	Surface rupture	IX	VIII
Pengawu	−0.9200	119.8509	Surface rupture	XI	VIII
Palupi	−0.9283	119.8528	Surface rupture	XI	VIII
Binangga	−0.9501	119.8590	Surface rupture	XI	VIII
Beka	−0.9803	119.8610	Surface rupture	XI	VIII
Bomba	−1.0070	119.8603	Surface rupture	XI	VIII
Kalungkutinggu	−1.0396	119.8632	Surface rupture	XI	VIII
Mantikole	−1.0649	119.8660	Surface rupture	XI	VIII
Balamoa	−1.0812	119.8645	Surface rupture	XI	VIII
Jono	−1.1132	119.8700	Surface rupture	IX	VIII
South Dolo	−1.1125	119.8726	Surface rupture	X	VIII
Poi	−1.1527	119.8811	Surface rupture	XI	VIII
Rogo	−1.1871	119.8893	Surface rupture	IX	VIII
Baluase	−1.1978	119.9041	Surface rupture	XI	VIII
Bolapapu	−1.4316	119.9841	Surface rupture	IX-X	VIII
Sungku	−1.4536	119.9862	Surface rupture	IX	VIII
Tuwa	−1.3474	119.9664	Surface rupture	IX-X	VIII
Palu	−0.9174	119.8503	Surface rupture	XI	VIII
Balane	−0.9498	119.8585	Surface rupture	XI	VIII
Dolo	−1.0043	119.8624	Surface rupture	XI	VIII
Pasaku	−1.0703	119.8642	Surface rupture	XI	VIII
Pakuli	−1.1969	119.9084	Surface rupture	XI	VIII
Sigi Regency	−1.3745	119.9746	Surface rupture	XI	VIII
Kulawi	−1.4290	119.9849	Surface rupture	XI	VIII
Panggang	−0,718,956	119,774,556	Tsunami	X	VII-VIII
Lolilondo	−0,747,154	119,780,534	Tsunami	X	VII-VIII-
Lolipesua	−0,769,695	119,788,484	Tsunami	X	VIII-IX
Lolisaluran	−0,843,634	119,818,903	Tsunami	XI	VIII-IX
Watusampu	−0,817,553	119,810,797	Tsunami	XI	VI-VIII
Silae	−0,874,983	119,834,851	Tsunami	X	VIII-IX
Ruko	−0,881,112	119,840,053	Tsunami	X	VII-VIII
Grandmall	−0,882,230	119,842,891	Tsunami	X	VIII
Mercure Hotel	−0,883,610	119,849,500	Tsunami	XI	VIII
TVRI	−0,885,830	119,862,850	Tsunami	XI	VIII

(*continued on next page*)

Table 4 (*continued*)

Location Name	Latitude	Longitude	EEEs type	ESI-07 scale	MMI Scale (USGS)
Nelayan	−0,863,900	119,878,140	Tsunami	XI	VIII
Tondo	−0,836,580	119,881,030	Tsunami	XI	VII-VIII
Citraland	−0,831,800	119,879,800	Tsunami	XI	VIII
Pergudangan	−0,823,540	119,882,350	Tsunami	XI	VIII
Kampung	−0,801,600	119,876,590	Tsunami	XI	VIII
Poltekes	−0,790,020	119,864,500	Tsunami	XI	VIII
Resort	−0,781,830	119,858,940	Tsunami	X	VIII
PLTU	−0,732,040	119,855,050	Tsunami	XI	VII-VIII
Pantoloan	−0,708,460	119,851,840	Tsunami	XI	VII-VIII
Ngada Wani	−0,695,010	119,840,330	Tsunami	XI	VIII
Labuan	−0,662,510	119,816,600	Tsunami	IX	VIII
TPI Lero	−0,629,120	119,811,520	Tsunami	X	VIII
Pasir Marana	−0,595,290	119,789,340	Tsunami	IX	VII-VIII
Tondo Lendi	−0,249,244	119,796,204	Tsunami	VIII	VIII
Mapaga	−0,231,051	119,802,160	Tsunami	VIII	VIII
Tipo	−0,860,717	119,828,593	Tsunami	IX	VIII
Donggala City	−0.663054	119.741313	Tsunami	VIII	VII
Loli Dondo	−0.731612	119.776100	Tsunami	VIII	VII-VIII
Loli Saluran	−0.783867	119.794095	Tsunami	VIII	VII-VIII
Watu Sampu	−0.822144	119.810032	Tsunami	XI	VIII
Tipo	−0.864574	119.829355	Tsunami	XI	VIII
Silae	−0.874580	119.834315	Tsunami	X	VIII
Lere	−0.885372	119.843401	Tsunami	VIII	VIII
Besusu Barat	−0.887457	119.860210	Tsunami	X	VII-VIII
Talise	−0.876266	119.873739	Tsunami	VIII	VIII
Tondo	−0.846571	119.880854	Tsunami	XI	VIII
Layana	−0.822159	119.887135	Tsunami	IX	VIII
Mamboro	−0.800542	119.878349	Tsunami	IX	VIII
Taipa	−0.778698	119.858686	Tsunami	X	VIII
Pantoloan	−0.710840	119.857660	Tsunami	IX	VIII
Wani	−0.693099	119.841543	Tsunami	X	VIII
Lero	−0.629011	119.812422	Tsunami	VIII	VIII
Tanjung Padang	−0.231612	119.803220	Tsunami	VIII	VIII
Lende	−0.185461	119.817232	Tsunami	VIII	VIII
Donggala	−0.785129°	119.796323°	Coastal Landslide	VII-VIII	VIII
Loli Sakuran	−0.828394°	119.811540°	Coastal Landslide	IX	VIII
Palu	−0.885368°	119.858772°	Coastal Landslide	VIII	VIII
Dupa	−0.789125°	119.863172°	Coastal Landslide	VIII-IX	VIII
Lubua	−0.703182°	119.845124°	Coastal Landslide	VIII-IX	VIII
Towaja	−0.630464°	119.811561°	Coastal Landslide	VIII	VIII
Oti	−0.407872°	119.843420°	Landslide	VIII	VIII
Sindue Tombusabora	−0.517535°	119.798222°	Landslide	IX	VIII
Lero	−0.614595°	119.927299°	Landslide	X	VII-VIII
Palu City	−0.863653°	119.948914°	Landslide	VIII	VII
Pinembani	−1.164369°	119.772294°	Landslide	VIII	VII
Pasaku	−1.155227°	119.863109°	Landslide	X	VII-VIII
Gumbasa	−1.288970°	119.974281°	Landslide	X	VII-VIII
Kulawi	−1.459889°	119.996733°	Landslide	X	VII
South Dolo	−1.327831°	119.913519°	Landslide	X	VIII
Beka	−0.992067°	119.865587°	Liquefaction	X	VII-VIII
Bomba	−1.008492°	119.855065°	Liquefaction	X	VII-VIII
Padende	−0.964024°	119.861789°	Liquefaction	X	VII-VIII
Binangga	−0.955197°	119.862420°	Liquefaction	X	VII-VIII
Kalukubula	−0.946776°	119.885591°	Liquefaction	X-XI	VII-VIII
Mpanau	−0.944210°	119.901693°	Liquefaction	X	VII-VIII
Biromaru	−0.958695°	119.914527°	Liquefaction	X	VII-VIII
Lolu	−0.963856°	119.918176°	Liquefaction	XI	VII-VIII
Jono Oge	−0.972822°	119.918509°	Liquefaction	X	VII-VIII
Sidera	−0.990422°	119.927512°	Liquefaction	X	VII-VIII
Karawana	−1.003675°	119.921391°	Liquefaction	X-XI	VII-VIII
Petobo	−0.935545°	119.908037°	Liquefaction	X	VII-VIII
Labuna	−0.1258°	119.8043°	Ground Cracks	X	VII-VIII
Balaesang	−0.1284°	119.8210°	Ground Cracks	X	VII-VIII
Lenden	−0.1615°	119.8234°	Ground Cracks	X	VII-VIII
Dampal	−0.2373°	119.7991°	Ground Cracks	X	VII-VIII
Tondo	−0.2635°	119.8205°	Ground Cracks	X	VII-VIII
Tamarenja	−0.4148°	119.8053°	Ground Cracks	X	VII-VIII
Sindue	−0.4444°	119.7686°	Ground Cracks	X	VII-VIII
Laone	−1.4056°	119.9778°	Ground Cracks	X	VII-VIII
Sadaunta	−1.3800°	119.9753°	Ground Cracks	X	VII-VIII
Tongkulawi	−1.4356°	119.9798°	Ground Cracks	X	VII-VIII
Boladangko	−1.4508°	119.9823°	Ground Cracks	X	VII-VIII
Jono Oge	−0.979115°	119.913483°	Ground Cracks	X	VII-VIII
Lolu	−0.958333°	119.920054°	Ground Cracks	X	VII-VIII
Mpanau	−0.949441°	119.923004°	Ground Cracks	X	VII-VIII
Petobo	−0.936172°	119.908564°	Ground Cracks	X	VII-VIII

(*continued on next page*)

Table 4 (*continued*)

Location Name	Latitude	Longitude	EEEs type	ESI-07 scale	MMI Scale (USGS)
Birobuli	−0.926121°	119.912982°	Ground Cracks	X	VII-VIII
Sidera	−0.993970°	119.921346°	Ground Cracks	X	VII-VIII
Karawana	−1.004775°	119.904477°	Ground Cracks	X	VII-VIII
Kotarindau	−0.995939°	119.900189°	Ground Cracks	X	VII-VIII
Langaleso	−0.993593°	119.903054°	Ground Cracks	X	VII-VIII

Indonesia.

The ESI-07 can be integrated with other traditional intensity scales as it solely relies on the damage observed in natural environments for regions like Indonesia or other Asian countries where they practice heterogeneous building codes. The reevaluation of macroseismic intensity using the EEEs for recent damaging earthquakes as well as historical earthquakes may help in the development of an empirical relationship between the earthquake magnitude and ESI intensity and the preparation of the ShakeMap based on the seismic intensity. This may provide a high-resolution seismic hazard estimation for Indonesia and other regions of the world. These EEEs and ESI-07 intensity data will be updated in the Istituto Superiore per la Protezione e la Ricerca Ambientale (ISPRA) site that can be further used for the future seismic hazard analysis for the study area.

The seismic hazard for an area depends upon the probability of earthquakes that will occur in an area within a specific time window and with the ground motion intensity exceeding a given threshold (Baker et al., 2021). The earthquake intensity determined from traditional intensity scales such as MM intensity scale, BMKG intensity scale, may saturate for intensity X to XII. It may be absent or too scarce in sparsely populated or desert areas. This can lead towards an erroneous seismic hazard estimation and the post disaster response. In that case the ESI 2007 scale should be used along with the other tradional intensity scales. For the intensity range between X and XII, the distribution and size of environmental effects, especially primary tectonic features, becomes the most diagnostic tool to assess the intensity level which may provide more accurate seismic intensity assessments. With more accurate intensity estimation by integrating the ESI-07 scale and traditional intensity scale together, the seismic risk can be assessed more precisely and included in such areas as building codes for standard buildings, designing larger buildings and infrastructure projects by engineers (Rasanen et al., 2021). Proper documentation of EEEs for the recent as well as historical earthquakes, will help to pinpoint the areas of enhanced hazards such as zone of surface rupture, liquefaction, landslides which will guide the engineers and policy makers towards a proper land use planning and deciding the insurance values.

8. Conclusions

An ESI-07 intensity map was produced and an ESI-07 intensity of (I_0 = X-XI ESI-07) was estimated for the epicentral area of the 2018 Sulawesi earthquake one of the most damaging earthquakes around Sulawesi in the recent past. For the 1996 Sulawesi earthquake, the ESI-07 was estimated to be VIII. The documentation of EEEs and intensity maps for the epicentral area is useful in seismic hazard assessment of the area, which has critical facilities like several ports, and airports.

By reassessing macroseismic intensity for the 28th September 2018 Sulawesi earthquake using the ESI-07 scale, we introduced the use of ESI-07 in Indonesia. The use of high-resolution satellite data with field data can complement each other for the macroseismic intensity estimation in developing countries where it is not possible to cover all the affected areas within a short period. In addition, it will help in rapid mapping of the EEEs to avoid the removal of EEEs in post-earthquake extreme climatic events such as heavy rain or during the post-disaster rescue operations.

The result suggests that the proper documentation of EEEs for damaging earthquakes of recent past and historical earthquakes in Indonesia can be useful for more accurate seismic hazard estimation. This will help in deciding the on-fault and off-fault deformation zone. A better idea of these zones will reduce the seismic hazard potential.

For accurate seismic hazard estimation on a local scale or regional scale, it is important for proper documentation of primary and secondary EEEs along with the ground motion data. In countries like Indonesia, which is continuously facing damaging earthquakes and has the potential to face similar earthquakes in the near future, information about EEEs can play an important role in land use planning and sustainable development as well as regional seismic hazard assessments in order to minimize the seismically induced damage.

Author contributions

SPN conceptualize the idea, compiled the data, and wrote the whole draft. AJ, TM, RP, and CL provide the field photos and corrected the draft. HM compiled the code and prepared the ESI-07 ShakeMap. AM, OG, KP helped in preparing the diagrams. HM, AMM, SP, and YSK corrected the draft.

Funding

The authors are thankful to Fundamental Research (PDU-No.641/UN4.1/KEP/2019) of Hasanuddin University, the Institute for Future City Studies at Tokyo City University, and the US National Science Foundation (StEER Network), the National Natural Science Foundation of China (42072250); National Institute of Water and Atmospheric Research (NIWA) through the New Zealand Government's Science Strategic Investment Fund (SSIF), grant number CARH2106. The authors are also thankful to the Korea Institute of Energy Technology Evaluation and Planning (KETEP) and the Ministry of Trade, Industry & Energy (MOTIE) of the Republic of Korea (No.20201510100020) for providing infrastructural facilities to carry forward this work.

Declaration of Competing Interest

The authors declare no competing interests.

Data availability

The Sentinel-2 imagery was obtained from Copernicus/ESA. MicMac software developed by IGN/ENSG (https://github.com/micmacIGN/micmac) was used for the processing of Sentinel-2 data. Optical displacement measurements from stacked profiles were acquired using StackProf software developed at IPGP by Laurent Pourchet (https://github.com/IPGP/stackprof). Topographic data were collected from the Center for Geospatial Information Management and Dissemination of Geospatial Information Agency (BIG), Indonesia, and the Center for Geospatial Information Management and Dissemination of Geospatial Information Agency (BIG), Indonesia. MM intensity data were collected from USGS https://earthquake.usgs.gov/earthquakes/eventpage/us1000h3p4/executive; Last accessed: 26th February 2022. Skala Intensitas Gempabhumi (SIG) (BMKG) were collected from https://www.bmkg.go.id/gempabumi/skala-intensitas-gempabumi.bmkg?lang=EN; Last accessed: 26th February 2022. 1996 Sulawesi earthquake MM intensity values were taken from USGS https://earthquake.usgs.gov/earthquakes/eventpage/usp00079zv/executive.

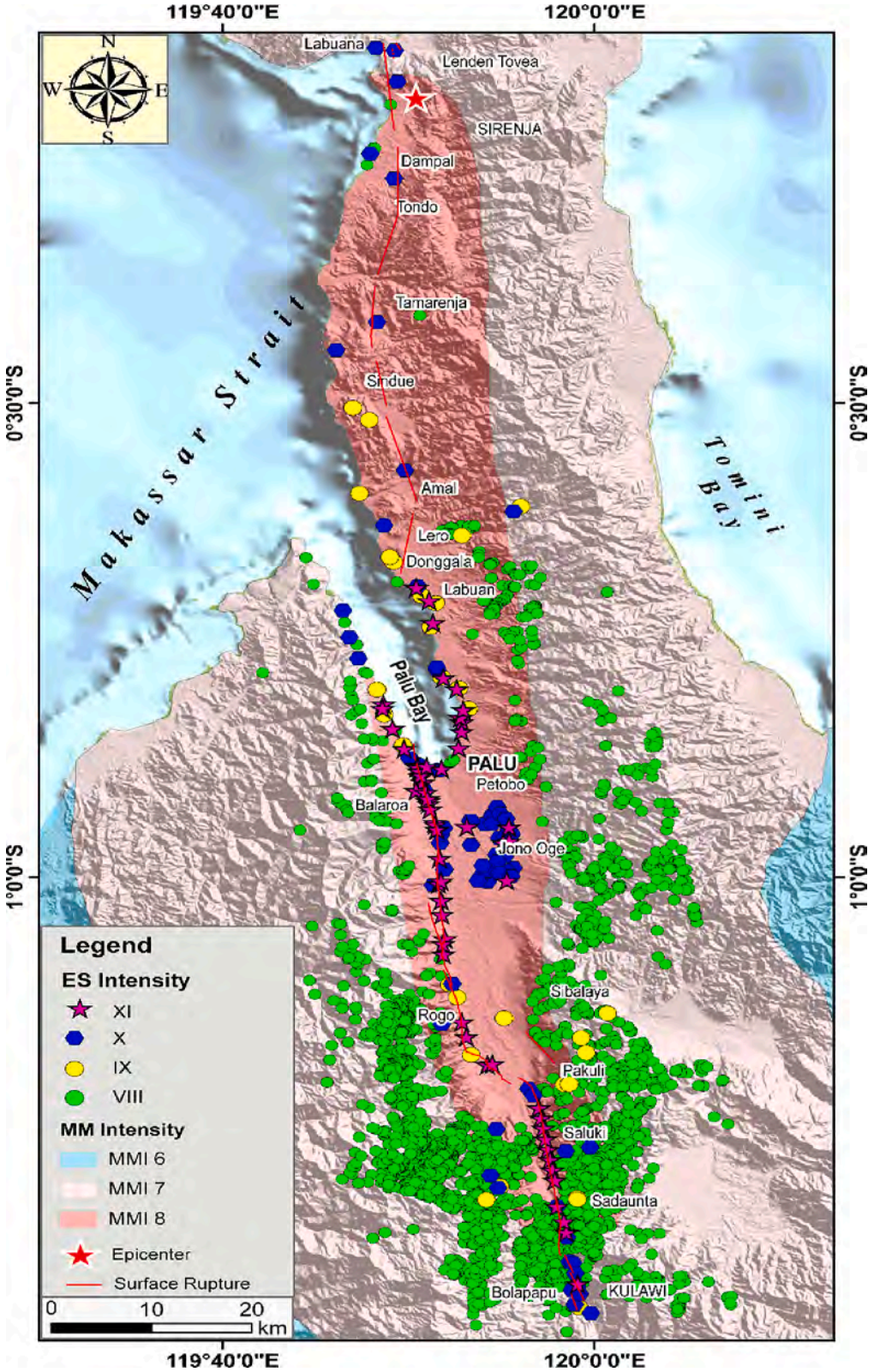

Fig. 15. ESI-07 map of the epicentral area showing distribution of ESI-07 values. The shaded line are the MM intensity contours taken from USGS.

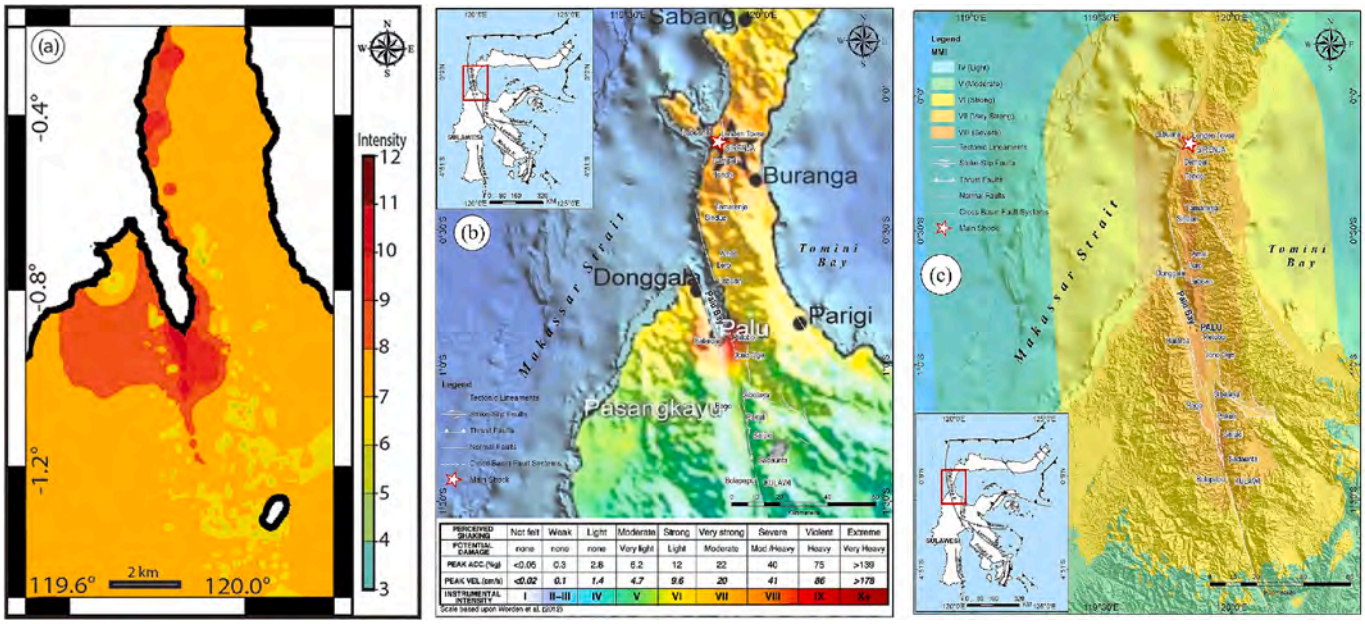

Fig. 16. ShakeMap for the 2018 Palu earthquake, (a) ESI-07 ShakeMap prepared from the ESI-07 values; (b) BMKG ShakeMap based on PGA values; (c) USGS ShakeMap taken from https://earthquake.usgs.gov/earthquakes/eventpage/us1000h3p4/executive.

Acknowledgments

The authors are thankful to funding agencies for providing the support to collect the field data. The authors are also thankful to USGS, and BMKG for providing useful information about the earthquake. The author HM is thankful to the Director, National Centre for Seismology, India, to allow HM to be part of this manuscript.

Appendix A. Supplementary data

Supplementary data to this article can be found online at https://doi.org/10.1016/j.enggeo.2023.107054.

References

Arias, A., 1970. A measure of earthquake intensity. In: Hansen, R.J. (Ed.), Seismic Design for Nuclear Power Plants. MIT Press, Cambridge MA, pp. 438–483.
Arikawa, T., Muhari, A., Okumura, Y., Dohi, Y., Afriyanto, B., Sujatmiko, K.A., Imamura, F., 2018. Coastal subsidence induced several tsunamis during the 2018 Sulawesi earthquake. J. Dis.r Res. 13 p.sc 20181201.
Bacqueset, G., de Michele, M., Foumelis, M., Raucoules, D., Lemoine, A., Briole, P., 2020. Sentinel optical and SAR data highlights multi-segment faulting during the 2018 Palu-Sulawesi earthquake (Mw 7.5). Sci. Rep. 10 (1), 1–11.
Baker, J., Bradley, B., Stafford, P., 2021. Seismic Risk. In: Seismic Hazard and Risk Analysis. Cambridge University Press, Cambridge, pp. 369–403.
Bellier, O., Sébrier, M., Beaudouin, T., Villeneuve, M., Braucher, R., Bourles, D., Siame, L., Putranto, E., Pratomo, I., 2001. High slip rate for a low seismicity along the Palu-Koro active fault in Central Sulawesi (Indonesia). Ter. No. 13 (6), 463–470.
Bradley, K., Mallick, R., Andikagumi, H., Hubbard, J., Meilianda, E., Switzer, A., Du, N., Brocard, G., Alfian, D., Benazir, B., Feng, G., 2019. Earthquake-triggered 2018 Palu Valley landslides enabled by wet rice cultivation. Nat. Geosci. 12 (11), 935–939.
Cilia, M.G., Mooney, W.D., Nugroho, C., 2021. Field insights and analysis of the 2018 Mw 7.5 Palu, Indonesia earthquake, tsunami and landslides. P. App. Geophy. 178 (12), 4891–4920.
Cipta, A., Omang, A., Supartoyo, Minarno, P.A., Solilkhin, A., Falah, F.N., Efendi, R., 2018. Anomali perilaku gelombang tsunami, in Di balik pesona Palu. ISBN: 978-602-9105-76-6. Badan Geologi, Kementerian Energi dan Sumber Daya Mineral, pp. 133–141.
Del Gaudio, V., Wasowski, J., 2011. Advances and problems in understanding the seismic response of potentially unstable slopes. Eng. Geol. 122 (1–2), 73–83.
Fan, X., Scaringi, G., Korup, O., West, A.J., van Westen, C.J., Tanyas, H., Hovius, N., Hales, T.C., Jibson, R.W., Allstadt, K.E., Zhang, L., 2019. Earthquake-induced chains of geologic hazards: patterns, mechanisms, and impacts. Rev. Geophys. 57 (2), 421–503.
Faris, F., Fathani, T.F., Wang, F., 2019. Report on the UNESCO Chair workshop on geoenvironmental disaster reduction 28th April-1st may, 2019, Palu-Jakarta, Indonesia. Geoenv. Dis. 6 (1), 1–6.
Fielding, E.J., Talebian, M., Rosen, P.A., Nazari, H., Jackson, J.A., Ghorashi, M., Walker, R., 2005. Surface ruptures and building damage of the 2003 Bam, Iran, earthquake mapped by satellite synthetic aperture radar interferometric correlation. J. Geophys. Res. 110 (B3).
Gomez, J.M., Madariaga, R., Walpersdorf, A., Chalard, E., 2000. The 1996 earthquakes in Sulawesi, Indonesia. Bull. Seismol. Soc. Am. 90 (3), 739–751.
Grünthal, G., Musson, R.M.W., Schwarz, J., Stucchi, M., 1998. European Macroseismic Scale 1998 (EMS-98). Cahiers du Centre Européen de Géodynamique et de Séismologie 15, Centre Européen de Géodynamique et de Séismologie, Luxembourg, p. 99. https://doi.org/10.2312/EMS-98. http://www.gfz-potsdam.de/EMS98.
Hall, R., Wilson, M.E.J., 2000. Neogene sutures in eastern Indonesia. J. Asia Earth Sci. 18 (6), 781–808.
Hamzah, L., Puspito, N.T., Imamura, F., 2000. Tsunami catalog and zones in Indonesia. J. Nat.Dis. Sc. 22 (1), 25–43.
Huayong, N., Hua, G., Yanchao, G., Blumetti, A.M., Comerci, V., Di Manna, P., Guerrieri, L., Vittori, E., 2019. Comparison of Earthquake Environmental Effects and ESI intensities for recent seismic events in different tectonic settings: Sichuan (SW China) and Central Apennines (Italy). Eng. Geol. 258, 105149.
Jaya, A., Nishikawa, O., Hayasaka, Y., 2017. LA-ICP-MS zircon U–Pb and muscovite K–Ar ages of basement rocks from the south arm of Sulawesi, Indonesia. Lith. 292, 96–110.
Jaya, A., Nishikawa, O., Jumadil, S., 2019. Distribution and morphology of the surface ruptures of the 2018 Donggala–Palu earthquake, Central Sulawesi, Indonesia. Eart. Plan. Sp. 71 (1), 1–13.
Jena, R., Pradhan, B., Beydoun, G., Sofyan, H., Affan, M., 2020. Integrated model for earthquake risk assessment using neural network and analytic hierarchy process: Aceh province, Indonesia. Geosci. Front. 11 (2), 613–634.
Keefer, D.K., 1984. Landslides caused by earthquakes. Geol. Soc. Am. Bull. 95 (4), 406–421.
Lario, J., Bardají, T., Silva, P.G., Zazo, C., Goy, J.L., 2016. Improving the coastal record of tsunamis in the ESI-07 scale: Tsunami Environmental Effects Scale (TEE-16 scale). Geol. Acta 14 (2), 179–193.
Larsen, I.J., Montgomery, D.R., Korup, O., 2010. Landslide erosion controlled by hillslope material. Nat. Geosci. 3 (4), 247–251.
Leeuwen, T.M.V., Muhardjo, T.M., 2005. Stratigraphy and tectonic setting of the Cretaceous and Paleogene volcanic-sedimentary successions in northwest Sulawesi, Indonesia: implications for the Cenozoic evolution of Western and Northern Sulawesi. J. Asian Earth Sci. 25 (3), 481–511.
Legendre, C.P., Tseng, T.L., Mittal, H., Hsu, C.H., Karakhanyan, A., Huang, B.S., 2017. Complex wave propagation revealed by peak ground velocity maps in the Caucasus Area. Seis. Res.Let. 88 (3), 812–821.
Lekkas, E.L., Andreadakis, E., Kostaki, I., Kapourani, E., 2013. A proposal for a new integrated tsunami intensity scale (ITIS-2012). Bull. Seismol. Soc. Am. 103 (2B), 1493–1502.
Lekkas, E.L., Mavroulis, S.D., 2015. Earthquake environmental effects and ESI 2007 seismic intensities of the early 2014 Cephalonia (Ionian Sea, western Greece) earthquakes (January 26 and February 3, Mw 6.0). Nat. Hazards 78 (3), 1517–1544.
Li, C., Liu, J., Ma, J., Su, G., Lan, J., Li, X., Ren, Z., Ran, H., 2022. Field observations of surface ruptures accompanying a tsunami and Supershear earthquake along a plate boundary strike-slip fault. Geol. Mag. 1–11.
Mason, H.B., Gallant, A.P., Hutabarat, D., Montgomery, J., Reed, A.N., Wartman, J., Irsyam, M., Prakoso, W., Djarwadi, D., Harnanto, D., Alatas, I., 2021a. Geotechnical

Reconnaissance: The 28 September 2018 M7. 5 Palu-Donggala. Indonesia Earthquake.
Mason, H.B., Montgomery, J., Gallant, A.P., Hutabarat, D., Reed, A.N., Wartman, J., Irsyam, M., Simatupang, P.T., Alatas, I.M., Prakoso, W.A., Djarwadi, D., 2021b. East Palu Valley flowslides induced by the 2018 MW 7.5 Palu-Donggala earthquake. Geomor. 373, 107482.
Mavroulis, S., Triantafyllou, I., Karavias, A., Gogou, M., Katsetsiadou, K.N., Lekkas, E., Papadopoulos, G.A., Parcharidis, I., 2021. Primary and secondary environmental effects triggered by the 30 October 2020, Mw= 7.0, Samos (Eastern Aegean Sea, Greece) earthquake based on post-event field surveys and InSAR analysis. Appl. Sci. 11 (7), 3281.
Medvedev, S., Sponheuer, W., Karník, V., Jena, V., 1964. Neue seismische Skala Intensity scale of earthquakes, 7. Tagung der Europäischen Seismologischen Kommission vom 24.9. bis 30.9. 1962. Jena, Veröff. Institut für Bodendynamik und Erdbebenforschung in Jena 77, 69–76.
Michetti, A.M., Esposito, E., Gürpinar, A., Mohammadioun, B., Porfido, S., Rogozhin, E., Serva, L., Tatevossian, R., Vittori, E., Audemard, F., Comerci, V., 2004. The INQUA scale. An innovative approach for assessing earthquake intensities based on seismically induced ground effects in natural environment. Special paper of the Italian Environment Protection and Technical Services Agency (APAT), Italy, Mem. Descr. Carta geol. d'Italia. LXVII.
Michetti, A.M., Esposito, E., Guerrieri, L., Porfido, S., Serva, L., Tatevossian, R., Vittori, E., Audemard, F., Azuma, T., Clague, J., Comerci, V., 2007. Intensity scale ESI 2007, Mem. Descrittive della Carta Geologica d'Italia. Rm 74, 53.
Mikami, T., Shibayama, T., Esteban, M., Takabatake, T., Nakamura, R., Nishida, Y., Achiari, H., Marzuki, A.G., Marzuki, M.F.H., Stolle, J., Krautwald, C., 2019. Field survey of the 2018 Sulawesi tsunami: inundation and run-up heights and damage to coastal communities. P. Appl.Geophy. 176 (8), 3291–3304.
Mittal, H., Wu, Y.M., Sharma, M.L., Lin, T.L., Yang, B.M., 2018. Shake maps generation for Delhi region using two different algorithms. In: Proceedings of the 16th Symposium on Earthquake Engineering. Department of Earthquake Engineering, Indian Institute of Technology, Roorkee, India, pp. 20–22.
Mittal, H., Wu, Y.M., Lin, T.L., Legendre, C.P., Gupta, S., Yang, B.M., 2019. Time-dependent ShakeMaps map for Uttarakhand Himalayas, India, using recorded earthquakes. Act. Geophy. 67, 753–763. https://doi.org/10.1007/s11600-019-00281-7.
Miyajima, M., Setiawan, H., Yoshida, M., Ono, Y., Kosa, K., Oktaviana, I.S., 2019. Geotechnical damage in the 2018 Sulawesi earthquake, Indonesia. Geoenv. Dis. 6 (1), 1–8.
Montgomery, J., Wartman, J., Reed, A.N., Gallant, A.P., Hutabarat, D., Mason, H.B., 2021. Field reconnaissance data from GEER investigation of the 2018 MW 7.5 Palu-Donggala earthquake. Data in Bri. 34, 106742.
Muhari, A., Imamura, F., Arikawa, T., Hakim, A.R., Afriyanto, B., 2018. Solving the puzzle of the September 2018 Palu, Indonesia, tsunami mystery: clues from the tsunami waveform and the initial field survey data. J. Disa. Res. 13 p.sc20181108.
Naik, S.P., Mohanty, A., Porfido, S., Tuttle, M., Gwon, O., Kim, Y.S., 2020. Intensity estimation for the 2001 Bhuj earthquake, India on ESI-07 scale and comparison with historical 16th June 1819 Allah bund earthquake: A test of ESI-07 application for intraplate earthquakes. Quat. Int. 536, 127–143.
Nappi, R., Porfido, S., Paganini, E., Vezzoli, L., Ferrario, M.F., Gaudiosi, G., Alessio, G., Michetti, A.M., 2021. The 2017, MD= 4.0, Casamicciola earthquake: ESI-07 scale evaluation and implications for the source model. Geosc. 11 (2), 44.
Natawidjaja, D.H., Daryono, M.R., Prasetya, G., Liu, P.L., Hananto, N.D., Kongko, W., Triyoso, W., Puji, A.R., Meilano, I., Gunawan, E., Supendi, P., 2021. The 2018 M w7. 5 Palu 'supershear' earthquake ruptures geological fault's multisegment separated by large bends: results from integrating field measurements, LiDAR, swath bathymetry and seismic-reflection data. Geophys. J. Int. 224 (2), 985–1002.
Omira, R., Dogan, G.G., Hidayat, R., Husrin, S., Prasetya, G., Annunziato, A., Proietti, C., Probst, P., Paparo, M.A., Wronna, M., Zaytsev, A., 2019. The September 28th, 2018, tsunami in Palu-Sulawesi, Indonesia: a post-event field survey. P. Appl. Geophy. 176 (4), 1379–1395.
Papadopoulos, G., Imamura, F., 2001. A proposal for a new tsunami intensity scale, ITS 2001. Proceedings, Session 5, 5–1.
Papanikolaou, I., Melaki, M., 2017. The Environmental Seismic Intensity Scale (ESI 2007) in Greece, addition of new events and its relationship with magnitude in Greece and the Mediterranean; preliminary attenuation relationships. Quat. Int. 451, 37–55.
Papathanassiou, G., Valkaniotis, S., Ganas, A., Grendas, N., Kollia, E., 2017. The November 17th, 2015 Lefkada (Greece) strike-slip earthquake: Field mapping of generated failures and assessment of macroseismic intensity ESI-07. Eng. Geol. 220, 13–30.
Patria, A., Putra, P.S., 2020. Development of the Palu–Koro Fault in NW Palu Valley, Indonesia. Geosc. Lett. 7 (1), 1–11.
Paulik, R., Gusman, A., Williams, J.H., Pratama, G.M., Lin, S.L., Prawirabhakti, A., Sulendra, K., Zachari, M.Y., Fortuna, Z.E.D., Layuk, N.B.P., Suwarni, N.W.I., 2019. Tsunami hazard and built environment damage observations from Palu City after the September 28 2018 Sulawesi earthquake and tsunami. P. Appl. Geophy. 176 (8), 3305–3321.
Pelinovsky, E., 1996, January. Tsunami of 1 January 1996 in Indonesia. In: Conference on Natural Disaster Reduction, 307–3.
Pelinovsky, E., Yuliadi, D., Prasetya, G., Hidayat, R., 1997. The 1996 Sulawesi tsunami. Nat. Hazards 16 (1), 29–38.
Porfido, S., Esposito, E., Vittori, E., Tranfaglia, G., Michetti, A.M., Blumetti, M., Ferreli, L., Guerrieri, L., Serva, L., 2002. Areal distribution of ground effects induced by strong earthquakes in the Southern Apennines (Italy). Surv. Geophys. 23 (6), 529–562.
Porfido, S., Esposito, E., Vittori, E., Tranfaglia, G., Guarrieri, L., Pece, R., 2007. Seismically induced ground effects of the 1805, 1930 and 1980 earthquakes in the Southern Apennines Ital. J. Geosci 126 (2),333-346.
Porfido, S., Alessio, G., Gaudiosi, G., Nappi, R., 2020. New perspectives in the definition/evaluation of seismic hazard through analysis of the environmental effects induced by earthquakes. Geosc. 10 (2), 58.
Prasetya, G.S., De Lange, W.P., Healy, T.R., 2001. The Makassar strait tsunamigenic region, Indonesia. Nat. Hazards 24 (3), 295–307.
Pribadi, S., Gunawan, I., Nugraha, J., Haryono, T., Erwana, Basri, C.A., Romadon, I., Mustarang, A., Heriyanto, Yatimantoro, T., 2018. Tsuanmi Survey on Palu Bay, 2018, Indonesia Geophysics. Climate and Meteorological Agency (BMKG).
PuSGeN, 2018. Post-event Studies of The 28 September 2018 Earthquake in Palu, Central Sulawesi (Kajian Gempa Palu Provinsi Sulawesi Tengah, 28 September 2018 (M7.4)), Pusat Perumahan dan Pemukiman, Balitbang PU.
PuSGeN, 2019. Progress Report of Post-2018 earthquake Studies forf Mapping The Palukoro Fault Hazard Zone (Laporan Pemetaan Zona Rawan Bencana Sesar Palukoro Pasca Gempa P28 Septemberr 28 2018). Center For Research And Development For Housing, Agency for Research and Development, Ministry of Public Works and Housing.
Putra, P.S., Aswan, A., Maryunani, K.A., Yulianto, E., Kongko, W., 2019. Field survey of the 2018 Sulawesi tsunami deposits. P. Appl. Geophy. 176 (6), 2203–2213.
Qi, T., Meng, X., Qing, F., Zhao, Y., Shi, W., Chen, G., Zhang, Y., Li, Y., Yue, D., Su, X., Guo, F., 2021. Distribution and characteristics of large landslides in a fault zone: A case study of the NE Qinghai-Tibet Plateau. Geomor. 379, 107592.
Rasanen, R.A., Marafi, N.A., Maurer, B.W., 2021. Compilation and forecasting of paleoliquefaction evidence for the strength of ground motions in the US Pacific Northwest. Eng. Geol. 292, 106253.
Rodríguez-Pascua, M.A., Pérez-López, R., Giner-Robles, J.L., Silva, P.G., Garduño-Monroy, V.H., Reicherter, K., 2011. A comprehensive classification of Earthquake Archaeological Effects (EAE) in archaeoseismology: application to ancient remains of Roman and Mesoamerican cultures. Quat. Int. 242 (1), 20–30.
Rodríguez-Peces, M.J., García-Mayordomo, J., Azañón, J.M., Arévalo, J.M.I., Pintor, J.J., 2011. Constraining pre-instrumental earthquake parameters from slope stability back-analysis: palaeoseismic reconstruction of the Güevéjar landslide during the 1st November 1755 Lisbon and 25th December 1884 Arenas del Rey earthquakes. Quat. Int. 242 (1), 76–89.
Sanchez, J.J., Maldonado, R.F., 2016. Application of the ESI 2007 scale to two large earthquakes: South Island, New Zealand (2010 M w 7.1), and Tohoku, Japan (2011 M w 9.0). Bull. Seismol. Soc. Am. 106 (3), 1151–1161.
Serva, L., Vittori, E., Comerci, V., Esposito, E., Guerrieri, L., Michetti, A.M., Mohammadioun, B., Mohammadioun, G.C., Porfido, S., Tatevossian, R.E., 2016. Earthquake hazard and the Environmental Seismic Intensity (ESI) scale. P. Appl. Geophy. 173 (5), 1479–1515.
Silva, P.G., Elez, J., Pérez-López, R., Giner-Robles, J.L., Gómez-Diego, P.V., Roquero, E., Rodríguez-Pascua, M.Á., Bardají, T., 2023. The AD 1755 Lisbon Earthquake-Tsunami: Seismic source modelling from the analysis of ESI-07 environmental data. Qut. Int. 651, 6–24.
Silva, P.G., Pérez-López, R., Rodríguez-Pascua, M.A., Giner, J.L., Huerta, P., Bardají, T., Martín-González, F., 2013. Earthquake environmental effects (EEEs) triggered by the 2011 Lorca earthquake (Mw 5.2, Betic Cordillera, SE Spain): Application of the ESI-07 macroseismic scale. Seismic Hazard, Critical Facilities and Slow Active Faults, pp. 237–240.
Silva, P.G., Elez, J., Giner-Robles, J.L., Rodríguez-Pascua, M.A., Pérez-López, R., Roquero, E., Bardají, T., Martínez-Graña, A., 2017. ESI-07 ShakeMaps for instrumental and historical events in the Betic Cordillera (SE Spain): an approach based on geological data and applied to seismic hazard. Quat. Int. 451, 185–208.
Silva, P.G., Rodríguez-Pascua, M.A., Giner Robles, J.L., Élez, J., Pérez-López, R., Davila, M.B.B., 2019. Catalogue of the geological effects of earthquakes in Spain based on the ESI-07 Macroseismic Scale: a new database for seismic hazard analysis. Geosc. 9, 334.
Socquet, A., Hollingsworth, J., Pathier, E., Bouchon, M., 2019. Evidence of supershear during the 2018 magnitude 7.5 Palu earthquake from space geodesy. Nat. Geosci. 12 (3), 192–199.
Socquet, A., Simons, W., Vigny, C., McCaffrey, R., Subarya, C., Sarsito, D., Ambrosius, B., Spakman, W., 2006. Microblock rotations and fault coupling in SE Asia triple junction (Sulawesi, Indonesia) from GPS and earthquake slip vector data. J. Geophys. Res. Solid Earth 111, B08409.
Song, X., Zhang, Y., Shan, X., Liu, Y., Gong, W., Qu, C., 2019. Geodetic observations of the 2018 Mw 7.5 Sulawesi earthquake and its implications for the kinematics of the Palu fault. Geophys. Res. Lett. 46 (8), 4212–4220.
Sopaheluwakan, J., Kadarusman, A., Priadi, B., Utoyo, H., 1995. The nature of basement rocks in Palu region, Central Sulawesi. The Newly found eclogite and its regional implication. In: Proceedings of Sixth International Congress on Pacific Neogene Stratigraphy and IGCP 355. PuspitekSerpong, West Java, Indonesia, pp. 77–83.
Tunas, I.G., Tanga, A., Oktavia, S.R., 2020. Impact of landslides induced by the 2018 Palu Earthquake on flash flood in Bangga River Basin, Sulawesi, Indonesia. J. Ecol. Eng. 21 (2).
Umar, M., Margaglio, G., Fitrayansyah, A., 2019. Post-tsunami survey of the 28 September 2018 tsunami near Palu Bay in Central Sulawesi, Indonesia: impacts and challenges to coastal communities. Int. J. Disa. Risk Red. 38, 101229.
Valkaniotis, S., Ganas, A., Barberopoulou, A., 2018. A preliminary report on the M7.5 Palu earthquake co-seismic ruptures and landslides using image correlation techniques on optical satellite data, 19th October 2018.
Velázquez-Bucio, M.M., Ferrario, M.F., Muccignato, E., Porfido, S., Sridharan, A., Chunga, K., Livio, F., Gopalan, S., Michetti, A.M., 2021. Environmental effects caused by the Mw 8.2, September 8, 2017, and Mw 7.4, June 23, 2020, Chiapas-

Oaxaca (Mexico) subduction events: comparison of large intraslab and interface earthquakes. Quat. Int. https://doi.org/10.1016/j.quaint.2021.11.028.
Villar-Vega, M., Silva, V., Crowley, H., Yepes, C., Tarque, N., Acevedo, A.B., Hube, M.A., Gustavo, C.D., María, H.S., 2017. Development of a fragility model for the residential building stock in South America. Earthquake Spectra 33 (2), 581–604.
Wald, D.J., Quitoriano, V., Heaton, T.H., Kanamori, H., Scrivner, C.W., Worden, C.B., 1999. TriNet "ShakeMaps": rapid generation of peak ground-motion and intensity maps for earthquakes in Southern California. Earthquake Spectra 15 (3), 537–556.
Wang, L., Gao, H., Feng, G., Xu, W., 2018. Source parameters and triggering links of the earthquake sequence in central Italy from 2009 to 2016 analyzed with GPS and InSAR data. Tectonophy. 744, 285–295.
Wardani, S.P.R., Muntohar, A.S., 2013. Lessons learned from the recent natural disasters in Indonesia. In: Geotechnical Predictions and Practice in Dealing with Geohazards. Springer, Dordrecht, pp. 47–59.
Wasowski, J., Keefer, D.K., Lee, C.T., 2011. Toward the next generation of research on earthquake-induced landslides: current issues and future challenges. Eng. Geol. 122 (1–2), 1–8.
Watkinson, I.M., Hall, R., 2017. Fault systems of the eastern Indonesian triple junction: evaluation of Quaternary activity and implications for seismic hazards. Geo. Soc. Lon. 441 (1), 71–120.
Widiyanto, W., Santoso, P.B., Hsiao, S.C., Imananta, R.T., 2019. Post-event field survey of 28 September 2018 Sulawesi earthquake and tsunami. Nat. Haz. Earth Sys. Sci. 19 (12), 2781–2794.
Williams, J.H., Paulik, R., Wilson, T.M., Wotherspoon, L., Rusdin, A., Pratama, G.M., 2020. Tsunami fragility functions for road and utility pole assets using field survey and remotely sensed data from the 2018 Sulawesi tsunami, Palu, Indonesia. Pure Appl. Geophys. 177 (8), 3545–3562.
Wood, H.O., Neumann, F., 1931. Modified Mercalli intensity scale of 1931. Bul. Seis. Soc. Ame. 21 (4), 277–283.
Wu, Y.M., Mittal, H., Huang, T.C., Yang, B.M., Jan, J.C., Chen, S.K., 2019. Performance of a low-cost earthquake early warning system (P-Alert) and shake map production during the 2018 M w 6.4 Hualien, Taiwan, earthquake. Seismol. Res. Lett. 90 (1), 19–29.
Wu, D., Ren, Z., Liu, J., Chen, J., Guo, P., Yin, G., Ran, H., Li, C., Yang, X., 2021. Coseismic surface rupture during the 2018 Mw 7.5 Palu earthquake, Sulawesi Island, Indonesia. GSA Bull. 133 (5–6), 1157–1166.
Yang, B.M., Huang, T.C., Wu, Y.M., 2018. ShakingAlarm: A nontraditional regional earthquake early warning system based on time-dependent anisotropic peak ground-motion attenuation relationships. Bull. Seismol. Soc. Am. 108 (3A), 1219–1230.
Yang, B.M., Mittal, H., Wu, Y.M., 2021. Real-time production of PGA, PGV, Intensity, and Sa ShakeMaps using dense MEMS-based sensors in Taiwan. Sens. 21 (3), 943.
Zhao, B., 2021. Landslides triggered by the 2018 Mw 7.5 Palu Supershear earthquake in Indonesia. Eng. Geol. 294, 106406.